HEATING AND CONFINEMENT IN THE ION CYCLOTRON RANGE OF FREQUENCIES ON THE DIVERTOR TOKAMAK ASDEX

K. Steinmetz, H. Niedermeyer, J.-M. Noterdaeme,
F. Wesner, F. Wagner, ICRH-, ASDEX-, NI-teams

IPP III / 130 January 1988

MAX-PLANCK-INSTITUT FÜR PLASMAPHYSIK

8046 GARCHING BEI MÜNCHEN

MAX-PLANCK-INSTITUT FÜR PLASMAPHYSIK

GARCHING BEI MÜNCHEN

HEATING AND CONFINEMENT IN THE ION CYCLOTRON RANGE OF FREQUENCIES ON THE DIVERTOR TOKAMAK ASDEX

K. Steinmetz, H. Niedermeyer, J.-M. Noterdaeme,
F. Wesner, F. Wagner, ICRH-, ASDEX-, NI-teams

IPP III / 130 January 1988

Submitted to NUCLEAR FUSION , January 1988.

Die nachstehende Arbeit wurde im Rahmen des Vertrages zwischen dem Max-Planck-Institut für Plasmaphysik und der Europäischen Atomgemeinschaft über die Zusammenarbeit auf dem Gebiete der Plasmaphysik durchgeführt.

HEATING AND CONFINEMENT IN THE ION CYCLOTRON RANGE OF FREQUENCIES ON THE DIVERTOR TOKAMAK ASDEX

K. Steinmetz, H. Niedermeyer, J.-M. Noterdaeme, F. Wesner, F. Wagner, J. Baeumler, G. Becker, W. Becker, H. S. Bosch, M. Brambilla, F. Braun, H. Brocken, G. Dodel[1], A. Eberhagen, R. Fritsch, G. Fussmann, O. Gehre, J. Gernhardt, G. v. Gierke, E. Glock, O. Gruber, G. Haas, J. Hofmann, F. Hofmeister, E. Holzhauer[1], A. Izvozchikov[2], G. Janeschitz, F. Karger, M. Keilhacker[3], A. Kislyakov[2], O. Klueber, M. Kornherr, P. B. Kotze[4], K. Lackner, G. Lisitano, E. van Mark, F. Mast, H. M. Mayer, K. McCormick, D. Meisel, V. Mertens, E. R. Mueller, H. Murmann, J. Neuhauser, A. Pietrzyk[5], W. Poschenrieder, S. Puri, H. Rapp, J. Roth, A. Rudyj, F. Ryter[6], F. Schneider, C. Setzensack, G. Siller, P. Smeulders[3], M. Soell[7], E. Speth, F. Soeldner, A. Staebler, K.-H. Steuer, O. Vollmer, H. Wedler, D. Zasche.

Max-Planck-Institut fuer Plasmaphysik,
EURATOM Association, D-8046 Garching, FRG

---

1 University of Stuttgart, FRG

2 Ioffe Institute, Leningrad, USSR

3 JET Culham, England

4 Nuclear Develop. Corp., Pretoria, South Africa

5 University of Washington, USA

6 CRPP, Lausanne, Switzerland

7 WTB Bernried, FRG

ABSTRACT

A summary of the experiments performed with ion cyclotron heating on ASDEX from November 1984 until March 1986 is given, and the most interesting results are reported and discussed in detail. Heating and confinement studies in the hydrogen second harmonic and hydrogen minority schemes ($P_{IC} < 2.6$ MW, $t_{IC} < 1.5$ sec) reveal a typical L-mode behaviour, i. e. a power dependent confinement degradation , which is rather similar to that found with neutral beam injection heating. ICRH is accompanied with a slightly improved particle and energy confinement compared to NI, which still holds when ICRH and NI are combined up to $P_{tot} \approx 4.5$ MW absorbed in the plasma. Particular efforts have been devoted to investigations of the second harmonic regime in H/D mixture plasmas of $n_H/n_e \approx 0.1$ to 1 which turns out to exhibit a high heating potential under reactor relevant plasma conditions. The achievement of H-mode transitions with ICRH alone in the hydrogen minority scheme at an absorbed RF power of about 1.1 MW supports the indications of a unique confinement structure with auxiliary heating in tokamaks which appears to be widely independent of the additional heating method. ICRH-specific impurity problems such as the strong release of iron from the vessel walls have been overcome by applying extensive in-situ wall carbonisation. The mechanisms responsible for the impurity generation have partly been identified and analyzed, however, the problem still remains to be solved. Impurities preferentially released from the ICRH antenna do not pose a problem.

INTRODUCTION

First experimental investigations on PLT, JFT-2M,TFR and ALCATOR C [1-7] have shown the potential of heating tokamak plasmas in the ion cyclotron range of frequencies (ICRH) performed either in the two-ion schemes (mode conversion and minority scenarios) or at the second harmonic resonance frequency of the majority ion species. Second harmonic heating appears particularly appealing since firstly, higher frequencies generally offer the possibility of applying wave guides or cavity antennae as launchers, and, secondly, experiments indicated that the wave absorption is already appreciable at the Ohmic temperature levels and might further improve with higher bulk plasma temperatures as achievable, for instance, either in large tokamaks like JET or in combined heating schemes with neutral beam injection. In particular, the second harmonic scheme is not expected to react very sensitive to variations of the plasma species mix which is an important feature with respect to reactor relevant plasmas. Various high-power ICRH experiments are now being conducted (JET, JT-60, TEXTOR, JFT-2M) [8-14] and lots of efforts are devoted to the application of high power ICRH to future machines like D III-D, ASDEX-UPGRADE, TORE SUPRA [15-17].

The paper gives a review of the ion cyclotron resonance heating experiments performed on ASDEX from November 1984 to March 1986 and compares some of the most interesting features of the RF scenarios with neutral beam heating in the same machine under optimized and reproducible plasma parameters. After a short reminder of the theoretical basis of ICRH and a brief description of the technical and experimental boundary conditions, experimental data on RF power absorption, heating and confinement in the L-mode, H-mode investigations, and profile features related to ICRH will be reported and

discussed. Additionally, a brief summary of the ICRH-specific impurity problems in case of a divertor plasma is given.

THEORETICAL BASIS

The principles of ICRH and the microscopic heating mechanisms itself have been identified and analyzed extensively since years [18-34]. Therefore, this section gives only a brief reminder of the theoretical basis of ICRH. In general, heating in the ion cyclotron range of frequencies is related to resonance layers , such as the ion cyclotron and the two-ion hybrid resonances, located within the plasma. In order to provide some wave electric field component in the correct (left-hand side) direction ICRH waves have to be applied to a fusion plasma either at the fundamental frequency to heat a hydrogen or a helium minority in a deuterium bulk plasma (D(H) , D(^{3}He)) or to work in the so-called mode conversion regime with high n_H/n_e values (n_H, n_e are proton and electron density, respectively), or have to be launched at the second harmonic resonance frequency of the bulk species, e. g. $2\Omega_{CH}$. All these schemes are based on launching fast magnetosonic waves (with the electric field polarized perpendicular to the magnetic field) excited by antennae located either at the outer or inner plasma boundary (the so-called low or high field side launching). Another type of ICRH, namely the ion Bernstein wave heating, with the electric field of the wave polarized parallel to B_0, has not been tried on Asdex.

A variety of theoretical models and numerical computations now exist to describe the RF properties of ICRH antennae and their field pattern, the propagation of the waves and the absorption of the RF power. In the literature, many antenna calculations based on slab models have been

considered [19-24]. Ray-tracing computations in the full tokamak geometry, which give essentially the first transit absorption, have been applied for years to various machines, but this method is only reliable in relatively large plasmas, where the WKB approximation is fullfilled [25-27]. Current investigations are mainly based on the 3-D solution of the full wave equations: Semi-analytic models have firstly been reported in [28,29]. Cold plasma approximations including collisional damping only are given in [30,31], while finite Larmor radius (FLR) effects have been added by [32]. Brambilla et al. [33] have considered both FLR effects and kinetic damping by solving the integro - differential equations. The integration of these models into tokamak transport codes is presently under way and should ultimatively allow both the determination of ICRH power deposition profiles allowing the direct evaluation of the transport properties of ICRF-heated plasmas .

EXPERIMENTAL CONDITIONS

The paper is related to ASDEX ICRH experiments performed until spring 1986 , before ASDEX was prepared to handle 10 sec long heating pulses with powers of up to 7 MW (4 MW ICRH and 3 MW NI). So far, ICRF operation was limited to 3 MW at the generators (frequency range : 30 to 115 MHz) for pulse lengths of about 2.5 sec due to the thermal properties of the antennae. Two conventional uncooled $\lambda/2$ loop antennae [35], consisting of two half-antennae each, were installed at the low magnetic field side, toroidally separated by 180 ^{o} from each other. Faraday screens provided the proper polarization of the radiated field pattern. Optically opaque screens as well as an optically open screen have been tested [36]. Each antenna was connected to one

generator thus forming an independent launching unit. A poloidal cross-section of ASDEX including the antenna arrangement is shown in Fig. 1 . In Ohmically preheated plasmas the distance between the separatrix and the Faraday screen, which affects the coupling and the metal impurity release, was typically about 5 cm, and about 3 cm in combination with NI , still in agreement with the requirements of full divertor operation. In these cases, the loading resistances of one half-antenna have been about 2 to 5 Ω, i. e. $R_L \approx 4$ to 10 Ω of one complete antenna, depending of the heating scheme. An overview of the ASDEX - RF system is given in [37-39]. ICRH power up to 2.6 MW (i.e. $P_{RF} >> P_{OH}$) for pulse lengths of up to 1.5 sec has been launched routinely. With carbonized vessel walls the RF pulse lengths were not limited by deleterious plasma effects but determined by either the flat top time of the plasma density and the current or by the pulse length of the neutral beam injection (NI) .

The launched RF power density averaged over the Faraday screen surface has been kept moderate at about 0.5 kW/cm^2, and is comparable to other fast wave experiments as summarized in Fig.2 [40]. Future machines of the NET type will require about 3 kW/cm^2 to limit the loss of blanket space. Higher voltage stand-off of the transmission line components or conceptually different antenna designs will be necessary to achieve this.

ICRH experiments on ASDEX have been performed at the hydrogen second harmonic frequency ($2\Omega_{CH}$, mostly f = 67 MHz), and at the fundamental frequency of hydrogen (33.5 MHz) in the hydrogen minority scheme (D(H)) in deuterium at toroidal magnetic fields of $B_0 \approx 2.2$ T which put the resonance layer close to the magnetic axis of the plasma [41-43].

Both ICRF scenarios have also been combined with NI under various

injection modes ($H^0 \rightarrow H^+$, $H^0 \rightarrow D^+$, $D^0 \rightarrow H^+$, $D^0 \rightarrow D^+$, tangential beam injection in co-direction) up to a total heating power of 4.5 MW absorbed by the plasma. It turned out that the combination of ICRH with NI has some obvious advantages: With a small amount of NI preheating (about 0.8 MW is sufficient), it is possible to apply the full ICRH power up to $P_{IC} \approx 2.6$ MW even without wall carbonisation. Without NI the ICRH power is limited to $P_{IC} \approx 1.2$ MW owing to ICRH-induced impurity radiation leading to major disruptions [41]. With NI, the power flux in the plasma is sufficiently increased so that higher radiation levels can be tolerated without causing disruptions. In addition, the ICRH power capability is enhanced in case of NI preheating : about 90% of the generator RF power can be transferred to the antennae with an ICRH power absorption coefficient of the plasma of about 70% (with OH target: about 80% and 60%, respectively).

Heating and confinement studies have been carried out in a wide parameter range : I_p = 250 to 450 kA, $\overline{n_e}$ = 2.5 to 9 10^{13} cm^{-3}, B_o = 1.7 to 2.7 T, P_{OH} = 0.2 to 0.5 MW, $P_{IC} < 2.6$ MW (power launched by the antennae) , $P_{NI} < 4.4$ MW . The target temperatures for ICRF heating typically are $T_{eo} \approx 600$ eV, $T_{io} \approx 500$ eV (at the standard density $\overline{n_e}$ = 4 10^{13} cm^{-3}) with Ohmic preheating , and T_{eo} = 1.2 -1.8 keV, $T_{io} <$ 2.5 keV with NI preheating. In order to reduce the ICRF induced metal impurity release extensive in situ carbon coating of the vessel wall [42] has been applied.

ICRF POWER ABSORPTION

The physics of coupling the fast wave to the plasma ions has clearly been identified by analysing the charge - exchange (CX) spectra of

hydrogen and deuterium measured both perpendicularly and parallel to the toroidal magnetic field. When applying hydrogen second harmonic launching to an Ohmically heated pure hydrogen plasma, the proton energy distribution in the central part of the plasma changes : the distribution becomes slightly non-maxwellian while the slope increases indicating an increase in T_i which is proportional to the ICRH power (Fig. 3a) . In the D(H) minority scenario, where wave damping is expected to take place essentially on the minority ions ($n_H/n_e \approx 5\%$) a strong perpendicular high-energy hydrogen tail develops during ICRH (Fig. 3b) with εtail temperaturesε of about 20 keV and extending up to particle energies of > 100 keV. The ion energy distribution of the deuterium (i. e. the bulk plasma), measured perpendicularly and parallel to B_o, remains thermal and shows, owing to the thermalization of the ICRF produced fast protons on the bulk species (electrons and ions), an increased ion temperature during ICRF heating .

The RF power absorption coefficient is determined as $\alpha = P_{IC}^{dep}/P_{IC}$, where P_{IC}^{dep} and P_{IC} are the RF power absorbed by the plasma and the power launched by the antennae, respectively. P_{IC} is calculated from the variation of the antenna loading resistances with and without plasma, R_p and R_v respectively : $P_{IC} = P_{RF} (1 - R_v / R_p)$. The global coupling is found to be sufficient, $P_{IC} = 0.8 - 0.9\ P_{RF}$, where P_{RF} is the net transmitted power (equal to forward minus reflected power), and depends obviously only weekly on plasma parameters. These values agree with theoretical estimates of the losses in the transmission lines and in the antennae circuits [35].

The effective power absorbed by the plasma , P_{IC}^{dep} , is determined by two different procedures :

a) via the rate of change of the plasma energy content following immediately an RF power step, where $P_{IC}^{dep} = dW_p/dt$. The reliability

of this procedure has been tested by analysing neutral beam injection pulses where the absorption coefficient can be calculated independently from a Monte-Carlo routine. Good agreement with beam deposition calculations is found (see Fig. 4).

b) via modelling the temporal behaviour of the change of the plasma energy content by $W_p(t) = W_p(OH) + \Delta W_p (1-\exp (-t / \tau_{inc}))$, where $\tau_{inc} = \Delta W_p / \Delta P_{AUX}^{dep}$. This ansatz gives a measure of the absorbed power as well as an estimate of the energy confinement time at infinetely large auxiliary heating power , the so-called incremental confinement time . The confinement aspects of this analysis will be discussed in the next section. The absorption coefficients determined by method b) agree rather well with those of the dW_p/dt-analysis. Fig. 4 gives a summary of the absorption coefficients. In Ohmic target plasmas at most 60 % of the launched power is absorbed by the central part of the plasma, $P_{IC}^{dep} \approx 0.6\ P_{IC}$, while with neutral beam heating the absorption increases slightly to $P_{IC}^{dep} \approx 0.7\ P_{IC}$. It is, however, not yet understood where the missing RF power is dissipated; there are experimental indications that part of that power might be transferred into the scrape-off layer and/or dissipated directly nearby the antennae structures [44]. Wave power losses at the stainless steel walls of the vessel have been estimated to stay less than 10%, while losses through the divertor slits are expected to account for 5%, at most , of the launched power [45] .So far, there is no quantitative theoretical explanation of these experimental observations. In the following, calculations of the global energy confinement times will contain $\alpha = 0.6$ and 0.7 for Ohmic and NI preheated discharges, respectively.

IMPURITY PROBLEMS

Although heating efficiency (defined as $\overline{n_e}\,\Delta T / P_{IC}$) and confinement features are found to be comparable or slightly better that those of NI heating, as shown in the following sections, ICRH exhibits some specific problems: The application of ICRH is, so far, always accompanied by a higher metal impurity content than observed with NI at the same power. In some experiments the metal impurities limited the maximum launchable RF power and / or the RF pulse length owing to disruptions. In JET, TFR, JFT-2M, and PLT (with ion Berstein wave heating) [44, 46-48] evidence has been found that part of the ICRH-induced metal impurity release takes place at or close to the antennae which might be related to particle acceleration by high RF electric fields excited in the near-field region of the antennae. However, erosion and sputtering of the vessel wall, even far away from the antennae (for instance, by fast ions and /or enhanced recycling) seem to play an important role, too.
Investigations on ASDEX [41, 43, 49] have evidenced a significant increase of the radiated power caused mainly by a higher iron concentration in the plasma resulting in centrally peaked radiation power density profiles ($p_{rad}(0) \approx 0.13$ W/cm^3 per MW RF power) which could be prevented only by wall carbonisation where then $p_{rad}(0) \approx 0.02$ to 0.05 W/cm^3 per MW (see Fig. 5). Neither the moderately improved particle confinement nor a reduction of impurity screening on account of changed plasma edge parameters [49, 63] have been found to be responsible for the observed metal impurity concentration. Impurity self-sputtering by oxygen and carbon can be experimentally excluded as possible production processes [49]. On the other hand, a clear anti-correlation between wave absorption in the confined plasma (excluding the plasma edge) and the impurity production has been

observed with suprathermal ions generated in the plasma edge region most likely caused by the RF electric fields building up due to the non-absorbed RF power circulating outside the s.o.l. [41, 42, 49]. Shifting the $2\Omega_{CH}$ resonance layer closer to the plasma periphery leads to higher edge localized fast ion fluxes and to higher radiation levels as well (Fig. 6). Additionally, the application of $2\Omega_{CH}$ launching to helium and deuterium plasmas with low hydrogen concentration which is related to an extremely low fast wave absorption, confirmes the deleterious influence of poor wave absorption within the main plasma. A quantitative explanation of the measured impurity level still remains to be given.

As the Faraday screen of the ICRH antennae is covered by TiC the antenna impurities can easily be discriminated from wall released impurities (Fe, Ni). The titanium fluxes from the antennae increase sensitively with decreasing density [50]. The total Ti fluxes, however, are small ($\Phi_{Ti} < 10^{17}$ atoms/s) compared to $\Phi_{FE} \approx 2.4 * 10^{19}$ atoms/s , so that the antennae contribution to the overall radiation can be neglected.

HEATING AND CONFINEMENT

HEATING EFFICIENCIES OF THE $2\Omega_{CH}$ and D(H) SCENARIOS

Carbonisation of the torus wall strongly reduces the metal impurity level during ICRH and allows the ICRH to operate up to maximum power without NI assistance. Thus, heating and confinement of purely ICRF heated plasmas could be studied.

Figure 7 displays the central line averaged electron density, the electron

temperature at different radial positions and the plasma energy content of a purely ICRF heated discharge. With the plasma in the L-mode the density can be kept constant by the feedback-control. A strong increase of $\overline{n_e}$ as observed on most limiter tokamaks has not been found. The electron temperature rises and becomes stationary during the 1 sec long ICRH pulse. The amplitude and the repetition time of the sawteeth increase with application of ICRH in a way similar to NI heating [51]; giant sawteeth as reported from JET [7,8] have never been observed on ASDEX.

The global ICRF heating efficiency , defined as increase of plasma energy content per launched MW RF power, $\Delta W_p/P_{IC}$, has been found to depend on the target plasma conditions, such as target temperature, species mix and impurity level:

The dependence of the ICRF heating efficiency on the species mix is illustrated in Fig. 8: It demonstrates that second hydrogen harmonic heating has also been successfully applied to H/D mixtures where conventional hydrogen minority heating (low-field side launching at the fundamental frequency) does no longer work. In H/D mixtures where the resonant species (H^+) is a relatively small fraction of the total particle content (10 to 20 %) the RF heating efficiency is found to be strongly enhanced beyond that of pure hydrogen operation probably owing to the isotope effect on confinement as observed also with OH and NI heating. At the lowest hydrogen concentrations ($n_H/n_e \approx 0.1$) the efficiency of the $2\Omega_{CH}$ scenario ($\approx$36 kJ/MW) compares well with that of the conventional D(H) minority scheme and is well above that of $2\Omega_{CH}$ heating in pure hydrogen ($\approx$21kJ/MW). Unsuccessful application of $2\Omega_{CH}$ to helium and pure deuterium plasmas clearly ruled out the possibility of 4th harmonic heating.

Figure 9 displays the global ICRF heating efficiencies of the $2\Omega_{CH}$

scenario versus the neutral beam power applied additionally to preheat the plasma , and compares conditions with and without carbonisation of the torus wall. When ICRH is applied to Ohmic plasmas the reduction of metal impurities and of the central radiation by carbonisation increases the RF heating efficiency by a factor of two thereby improving the energy confinement by about 20 to 30%. With NI preheating the effect of carbonisation becomes less important. In combining ICRH plus NI an interesting question is whether the RF heating efficiency becomes improved with increasing ion target temperature or by coupling of the wave to the fast beam ions. As shown in Fig. 9, the increase of T_i - when carbonisation is applied - due to hydrogen beam preheating improves the ICRF efficiency by about 25 % , from about 20 kJ/MW (w/o NI, $T_{io} \approx 0.5$ keV) to about 25 kJ/MW at $P_{NI} = 3.5$ MW ($T_{io} \approx$ 2.2 keV) in pure hydrogen plasma.

Furthermore, some coupling of the IC wave to the beam ions is observed (e.g. in CX-spectra [52]), but to an extent which is not sufficient to improve the heating significantly: Comparing discharges of $H^0 \rightarrow D^+$ and $D^0 \rightarrow H^+$ injection together with $2\Omega_{CH}$ launching the RF heating efficiency turns out to be independent (within 10%) of the beam species , and indicates clearly bulk heating as the main ICRF absorption scenario ($2\Omega_{CH}$ is not expected to couple to the injected D^+ - ions). Heating by direct absorption of the wave by the beam ions is found experimentally to contribute less than 10% [42], i. e. less than predicted by theory [53], which might be related to the fact that only a hot beam component perpendicular to the toroidal magnetic field can act as an effective absorber for the fast wave. However, on ASDEX tangential beam injection is applied with only a small component of scattered hot ions perpendicular to B_o.

Although the global heating efficiency (to be determined intrinsically by

wave absorption and energy confinement) cannot be compared directly with the computed single pass absorption of the launched ICRF power, it is interesting to note that ray-tracing computations predict a strong increase of the single pass absorption with the plasma beta. Based on ASDEX parameters the single pass absorption is expected to increase by a factor of three [54] from about 14 % to 43 % when raising the ion temperature from 0.5 keV to 3 keV. Experimentally, an enhancement factor of about 1.2 with respect to the total absorption and the global heating efficiency is measured.

Electron and ion heating is observed in both the $2\Omega_{CH}$ and the D(H) schemes. Central electron heating (Fig. 10 a), as derived via the initial slope of the sawteeth, is found to be significantly higher in the minority mode than at $2\Omega_{CH}$ which agrees, at least qualitatively, with theoretical expectation. Recent computations solving the full-wave equations [33] predict a rather low direct electron heating by ICRH, even for the minority scheme on ASDEX: The fraction of the absorbed power due to H cyclotron damping is calculated to about 71%, D harmonic damping accounts for about 15%, while the total direct electron heating (electron transit time magnetic pumping, electron Landau damping, stochastic Bernstein wave damping) takes only 11%.

The global electron heating efficiency (which includes energy transport) $\eta_e = \overline{n_e}\, \Delta T_{eo} / P_{IC}$ of about 4.0 and 1.8 10^{13} eV/kWcm^3 for D(H) and $2\Omega_{CH}$ (pure H-plasma) respectively, is also higher in the minority scheme which, however, is partly related to the better confinement properties of deuterium plasmas. Figure 10 b presents the ion heating at $P_{IC} < 0.7$ MW where the minority regime exhibits an efficiency as high as the NI H-mode (4.2 10^{13} eV/kWcm^3 [55]) in agreement with the observed non-degraded energy confinement in the

low power D(H) scheme (see Fig. 12). The good energy confinement of D(H) heating in ASDEX is discussed in the next section.

The success of RF heating experiments has often been characterized by the so-called global heating efficiency or global heating rate, defined as $\eta = \overline{n_e} (\Delta T_{eo} + \Delta T_{io}) / P_{IC}$. In order to compare different machines with different plasma conditions it is useful to normalize the data to the plasma volumes V_p and the target (i.e. Ohmic) confinement times $\tau_E(OH)$. Figure 11 gives an overview of some experimental results, taken from the literature, where now the normalized heating rates are dimensionless (as they should be):

$$\eta^* = \overline{n_e} (\Delta T_{eo} + \Delta T_{io}) V_p / (P_{IC} \tau_E) .$$

Within a factor of two η^* (which does not take profile effects into account) is found to be rather independent of the configuration of the experiment, the plasma size, the RF power and the heating scheme. No significant systematic differences are observed for the RF scenarios (hydrogen second harmonic, hydrogen minority, mode conversion, ion Bernstein wave heating) and neutral beam injection heating.

CONFINEMENT OF D(H) AND $2\Omega_{CH}$ HEATING

The key problem of tokamak research is the accessibility of confinement regimes with τ_E-values sufficiently high to reach ignition. Figure 12 displays the energy confinement of the D(H) and $2\Omega_{CH}$ schemes. Obviously, $2\Omega_{CH}$ and D(H) heating behave quite differently with respect to the energy confinement at low RF power: For $P_{IC} < 0.55$ MW the minority scenario shows a significant better ion and electron heating than the $2\Omega_{CH}$ scheme which is consistent with the higher τ_E-values observed with D(H). An interesting delay in the onset of the transition from Ohmic to L-mode confinement is observed for D(H) heating (see

Fig.12). τ_E remains constant (in some cases even better than the OH-values) up to $P_{IC} \approx 0.55$ MW (about 1.4 times the Ohmic heating power). At present, we cannot give a plausible explanation of this interesting feature. There is no immediate indication from the development of the plasma profiles when we compare the D(H) with the $2\Omega_{CH}$ or the NI data at low power.

Figure13 summarizes the confinement of auxiliary heating by ICRH, ICRH+NI, and NI obtained on ASDEX. The confinement times are normalized to the Ohmic phases in order to eliminate isotope effects due to varying plasma species mix. At RF power $P_{IC} > 0.6$ MW the plasma generally reacts with degraded confinement : Both RF scenarios essentially follow an L-mode scaling while the D(H) scheme appears to be slightly better than $2\Omega_{CH}$. The W_p vs P_{tot} data (Fig. 14) both of the D(H) and the $2\Omega_{CH}$ schemes can be fitted by an offset-linear scaling [56] of the form $W_p = W_p(OH) + P_{IC}^{dep} \tau_{inc}$ with incremental energy confinement times $\tau_{inc} = \Delta W_p^{IC} / \Delta P_{IC}^{dep}$ slightly higher for D(H) ($\tau_{inc} \approx 40$ ms) than for $2\Omega_{CH}$ heating ($\tau_{inc} \approx 32$ ms). The diamagntically measured ICRH gross energy confinement times $\tau_E = W_p / (P_{OH}' + \alpha P_{IC})$ are systematically in excess (by about 30%) of those obtained with NI; the differences, however, are still within the combined error bars. For comparison, Fig. 15 shows the increase of the plasma energy content W_p due to an NI pulse and a subsequent ICRH pulse of about the same power (both in the L-mode). The W_p trace is supplemented by the central line averaged electron density and four T_e traces at different radial positions. The increase of W_p with ICRH is slightly higher indicating an L-type confinement weekly superior to that of beam heated discharges. The systematic improvement of the confinement with ICRH with respect to NI is supported by the observation that with ICRH particle confinement does only weakly

degrade with respect to the Ohmic phase, which is indicated by the constancy of the plasma density when switching on ICRH (with NI $\overline{n_e}$ decreases in the L-mode), and more obvious from the only slightly enhanced impurity transport (which is significantly increased during NI). Figure 16 illustrates the decay (i. e. transport) times of TiXX, injected into the plasma by laser blow-off, indicating similar trends for impurity / particle transport and energy confinement. In comparison to NI the impurity transport analysis for ICRH suggests an enhancement of the inward drift rather than a reduction of the diffusion coefficient . It is not yet clear whether the improved particle confinement and the absence or reduction of plasma rotation during ICRF heating affects the confinement degradation. Besides the characteristic L-type scaling of τ_E with power (Fig. 13) the energy confinement of ICRF heated plasmas scales linearly with plasma current and is independent of the line averaged electron density (Fig. 17), thus exhibiting many global similarities to the confinement properties of NI heated plasmas in ASDEX [51, 55, 57].

For $P_{IC} > 0.7$ MW the ICRH data can be fitted either by an offset-linear scaling, as described above, or by a power dependent form :

$$\tau_E \propto 1.74\ I_p(MA)\ P_{tot}^{-0.45}(MW)$$

with

$$\tau_E\ (\ D(H)\ )\ /\ \tau_E\ (\ 2\Omega_{CH}\ ) \approx 1.25$$

CONFINEMENT WITH COMBINED ICRH + NI

Both RF heating schemes have been combined with neutral beam injection up to a total heating power of about 4.5 MW absorbed by the plasma ($P_{NI} < 3.5$ MW, $P_{IC} < 2.6$ MW) which is about 45 times the residual Ohmic power during additional heating. Figure 18a) displays the traces

of the plasma energy content, the line averaged central electron density and the electron temperature at different radial positions for the combination of NI plus ICRH at about equal heating power. Since the density is kept constant during the ICRH pulse the additional plasma energy content is due to an increase in electron and ion temperature as shown in Fig. 18b, where T_i is measured by means of charge-exchange recombination spectra of O VIII radiating close to the plasma centre. In the combined heating scenario the degradation of confinement at high power also appears to be less severe than with NI alone. In particular, the ICRH plus NI data (Fig. 13) at high power indicate the existence of a substantial residual energy confinement which is about half the Ohmic value. The corresponding figures of this τ_E - plateau $\tau_E / \tau_E(OH) =$ 0.43 to 0.5, where $\tau_E = W_p / (P_{OH'} + 0.85\ P_{NI} + 0.7\ P_{IC})$ without correction for central radiation, are consistent with a τ_{inc} - analysis modelling the increase of the plasma energy content ΔW_p following an RF power step by $W_p = W_p(0) + \Delta W_p^{IC} (1 - \exp (- t / \tau_{inc}))$. The so calculated incremental confinement times are marked by the shadowed region in Fig. 13 and agree reasonably with the experimental points at highest power supporting strongly a τ_{inc} - model [58]. In our experiments, W_p has been increased by a factor of about 5, from 26 kJ at P_{OH} = 0.4 MW to 123 kJ at P_{tot} = 4.4 MW. The improved confinement of the combined heating scheme is also supported by the observation of a reduced impurity transport (see ICRH + NI data in Fig. 16).

THE H-MODE WITH ICRH

Our H-mode investigations , with ICRH either applied alone or together with NI, were based on an H-mode recipe which has been developed

during NI experiments on ASDEX [59]. The optimum standard H-mode conditions are: Clean deuterium plasmas of Z_{eff} = 1-1.5 in the single-null divertor configuration where the plasma is shifted vertically up by about 4 cm (corresponding to 2 times the n_e and T_e falloff lengths of the scrape-off layer). Thus the ion grad-B-drift is directed to the X-point (i. e. upwards) yielding the lowest power limit for achieving the H-mode.

With D(H) heating, for the first time [60], H-mode transitions have been achieved reproducibly with ICRH alone (carbonised vessel walls) at an RF power of $P_{IC} \approx 1.7$ MW launched by two antennae.

An example is shown in Figure 19 where the minority concentration has been controlled to about $n_H/n_e \approx$ (2-4) %. In all discharges of this type H-modes have been reached just marginally and developed out of L-phases with sawteeth. The H-transitions show all characteristic features like a distinct drop in the energy flux flowing into the divertor (monitored by the H_α light in the divertor), rising $\overline{n_e}$ (due to improved particle confinement), enhanced plasma energy content (owing to improved energy confinement), and frequent ELMs (edge localized MHD modes). Another important observation is the edge electron temperature pedestal of $T_e(a) \approx 300$ eV in comparison to the profile prior to the H-transition (Fig. 19), which develops similarly to the behaviour found with NI heating alone.

With respect to the absorbed RF power, $P_{IC}^{dep} \approx$ 1MW, the threshold power for achieving the H-transition appears to be roughly equal to that found with pure NI heating. Figure 20 displays the development of the H-mode with pure D(H) heating when raising the RF power. At P_{IC} = 1 MW a typical L-mode behaviour is observed, monitored e. g. by the reduced electron density and by the sawtooth modulations of the H_α signal in the divertor (Fig. 20a). Increasing the launched RF power to P_{IC} = 1.5 MW

almost each sawtooth triggers - due to the power flux to the plasma edge - a very short H-transition (marked by arrows in Fig. 20b), while with P_{IC} = 1.7 MW the H-mode is achieved marginally.

During short ELM-free phases (H^* , see insert of Fig. 19) the boundary layer contracts sharply as it is well known from NI investigations. The sudden increase of the effective distance between antennae and plasma reduces the antenna coupling by about 40 to 50%, from about 2.7 Ω to 1.8 Ω (Fig. 21), so that the resulting voltage increase in the RF vacuum transmission lines (the RF power is kept constant !) has always caused a voltage breakdown terminating at least one of the generators. The reduction of the antenna loading resistance can be understood in terms of the variation of the effective distance between antenna and separatrix, and alterations of the density fall-off length close to the antenna [45]. Unfortunately, this technical constaint could not be avoided so far. In order to overcome it a higher voltage stand-off capability is required which will now be available on ASDEX. Present investigations on our test bed indicate voltage stand-off capabilities of up to 90 kV [61].

Although a data base of ICRF H-mode confinement which could be compared with NI heating is not yet available because of the technical problems which hampered these studies it has been demonstrated that the H-mode is accessible with ICRH alone, which is of significant importance both for the understanding of confinement physics and the choice of the RF heating in forthcoming experiments. The feasiliby of the H-mode with pure ICRH has also successfully been demonstrated on JFT-2M [62].

PROFILE FEATURES OF ICRH

Rather narrow power deposition profiles are expected theoretically for ICRF heating [33]. In fact, ICRH (with the resonance layer close to the plasma axis) is accompanied by T_e profiles which are strongly peaked on axis. Figure 22 illustrates the developement of $T_e(r)$ with RF power : The higher the RF power the steeper the T_e profile, in particular inside the sawtooth mixing radius ($r_{sm} \approx r_{q=1}\sqrt{2}$), until, at higher power, the profile becomes essentially triangular. During ICRH, in particular in the D(H) scheme the electron temperature and pressure profiles are much more peaked inside r_{sm} than in case of NI, as shown in Fig. 23 where the T_e profiles have been normalized at a radial position outside the sawtooth mixing radius. This holds also for the combination of ICRH+NI (Fig. 24) where the energy confinement improves by about 30%, at the same total power, compared to NI heating alone. As far as $n_e(r)$ is concerned, the electron density profiles remain essentially unchanged at the plasma boundary (between separatrix and antenna) [42, 63] whereas $n_e(r)$ becomes slightly peaked with ICRH in the plasma centre. Whether the peakedness of the profiles (as observed in a much stronger way in the ' good ' pellet regimes with improved confinement [64]) during ICRH is directly related to the slight improvement of τ_E is not yet understood.

We have attempted to test the effect of temperature profile shaping by varying the ICRH power deposition through either shifting the $2\Omega_{CH}$ resonance layer radially while maintaining q_a = 3.3 = constant, or by working with two resonance layer positions simultaneously, excited by two antennae operating at different frequencies (67 MHz for $r_{res} \approx$ 0 cm, and 61.9 MHz for $r_{res} \approx a/2$ = 20 cm). Combined with a small amount of NI heating (P_{NI} = 0.4 MW) the RF power of each antenna has

been varied (but P_{IC}^{tot} = 0.9 MW = constant): In case of primarily off-axis RF power deposition neither a significant alteration of the electron temperature and pressure profiles outside q=1 nor a change of the gross energy confinement time with respect to on-axis deposition have been observed. However, the effective variation of the ICRH electron power deposition profile including transport effects with on/off-axis ICRH is difficult to calculate. No information is so far available on ASDEX of the ion temperature profiles with ICRH under these conditions, which would be of great interest, in particular, because $2\Omega_{CH}$ directly heats essentially the bulk ions and much less the electrons. In fact, investigations reported from JET [9] indicate a relatively strong flattening of $T_i(r)$ with off-axis deposition.

SUMMARY AND CONCLUSIONS

In summary, present experiments on heating in the ion cyclotron range of frequencies in tokamaks reveal a significant progress towards scenarios sufficiently reliable and efficient to reach ignition [65]. On ASDEX it has been shown that NI and ICRH give rise to the same L and H-mode confinement structures. The dominant confinement regimes of auxiliary heated plasmas are found to be independent of the heating method. Additional aspects of NI, like particle and momentum transfer, or the development of anisotropic ion energy distributions, are of minor importance. Heating in the second harmonic regime, particularly in H/D mixtures (see Fig. 8), has been found as efficient as minority heating, and is, because of its wide insensitivity to the species mix, of particular relevance for application to fusion reactor conditions.

Despite the high potential of ICRH to heat large tokamaks some

ICRH-specific physics problems still remain to be solved : To improve our understanding of the processes responsible for impurity generation, more emphasis has to be put on investigations clarifying the interaction between RF waves, the plasma boundary and the walls of fusion devices. These studies will be of particular interest in terms of the problems accompanied and , of course , related to all heating regimes of improved particle confinement like ICRH plus counter NI, pellet refuelling and H-mode.

The data basis for other critical issues, such as the density limit and beta limit with ICRH are scarce. Concerning impurity problems, no significant increase of the density limit with ICRH power, as compared to NI heating, has so far been observed. The successful application of ICRH heating to plasmas close to the beta limit is not yet proven and is another important topic of further investigations.

ACKNOWLEDGEMENTS

The excellent support of the ICRH, ASDEX, and NI operation groups are gratefully acknowledged.

REFERENCES

[1] HWANG, D., BITTER, M., BUDNY, R., et al., in Plasma Physics and Controlled Nuclear Fusion Research (Proc. 9th Intern. Conf. Baltimore, 1982) Vol. 2, IAEA, Vienna (1983) 3.

[2] HOSEA, J., BRETZ, N., CAVALLO, A., et al., in Heating in Toroidal Plasmas (Proc. 3rd Joint Varenna-Grenoble Intern. Symp. Grenoble, 1982) Vol. 1, CEC (1982) 213.

[3] MATSUMOTO, M., KIMURA, H., ODAJIMA, K., et al., Nucl. Fusion 24 (1984) 283.

[4] ODAJIMA, K., MATSUMOTO, H., KIMURA, H., et al., in Heating in Toroidal Plasmas (Proc. 4th Intern. Symp. Rome, 1984) Vol.1, CEC (1984) 243.

[5] Equipe TFR, in Heating in Toroidal Plasmas (Proc. 3rd Joint Varenna-Grenoble Intern. Symp. Grenoble, 1982) Vol. 1 (1982) 225.

[6] ADAM, J., equipe TFR, Plasma Physics and Contr. Fusion 25 (1984) 165.

[7] PORKOLAB, M., BONOLI, P., CHEN, K., et al., in Plasma Physics and Controlled Nuclear Fusion Research 1986 (Proc. 11th Intern. Conf. Kyoto, 1986), Vol. 1, IAEA, Vienna (1987) 509.

[8] REBUT, P.H., ALTMANN, H., ANDERSON, R.J., et al., ibid, 31.

[9] JACQUINOT, J., ALTMANN, H., ANDERSON, R.J., et al., ibid, 449.

[10] YOSHIKAWA, M., ABE, T., AIKAWA, H., et al., ibid, 11.

[11] VANDENPLAS, P.E., DELVIGNE, T., DESCAMPS, P., et al., ibid, 485.

[12] WEYNANTS, R. R., JADOUL, M., MESSIAEN, A.M., et al., in Controlled Fusion and Plasma Physics (Proc. 14th Europ. Conf. Madrid, 1987) Vol. 11 D, Part I, EPS (1987) 197.

[13] ODAJIMA, K., FUNUHASHI, A., HOSHINO, K., et al., in Plasma Physics and Controlled Nuclear Fusion Research 1986 (Proc. 11th Intern. Conf. Kyoto, 1986), Vol. 1, IAEA, Vienna (1987) 151.

[14] WATARI, T., OHKUBO, K., AKIJAMA, R., et al., ibid, 495.

[15] LUXON, J. L., BROOKS, N.H., DAVIS, L.G., et al., in Controlled Fusion and Plasma Physics (Proc. 11th Europ. Conf. Aachen, 1983) Vol. 7D, Part I, EPS (1983) 99.

[16] AUG team, heating teams, Application for EURATOM Priority Support of Additional Heating for ASDEX Upgrade, Phase I and Phase II, report IPP 1/237 (1985), Max-Planck-Institut fuer Plasmaphysik, Garching, and
WESNER, F., NOTERDAEME, J.-M., BAEUMLER, J., et al., in Controlled Fusion and Plasma Heating (Proc. 13th Europ. Conf. Schliersee, 1986) Vol.10 C, Part II, EPS (1986) 173.

[17] ADAM, J., AYMAR, R., BANNELIER, P., et al., Implementation of Additional Heating on TORE SUPRA, Fontenay-aux-Roses,Association EURATOM CEA (1983).

[18] STIX, T. H., The Theory of Plasma Waves, McGraw Hill, NY (1962).

[19] WEYNANTS, R. R., MESSIAEN, A.M., LEBLUD, C., VANDENPLAS, P.E., in Heating in Toroidal Plasmas (Proc. 2nd Joint Grenoble-Varenna Intern. Symp. Como, 1980) Vol.1, CEC (1980) 487.

[20] THEILHABER, K., JACQUINOT, J., Nucl. Fusion 24 (1984) 541.

[21] RAM, A., BERS, A., Nucl. Fusion 24 (1984) 679.

[22] FUKUYAMA, A., NISHIYAMA, S., ITOH, K., ITOH, S.-I., Nuclear Fusion 23 (1983) 1005.

[23] APPERT, K., HELLSTEN, T., VACLAVIK, J., VILLARD, L., Comp. Phys. Comm. 40 (1986) 73.

[24] BRAMBILLA, M., KRUECKEN, T., in Controlled Fusion and Plasma Heating (Proc. 13th Europ. Conf. Schliersee, 1986) Vol.10 C, Part II, EPS (1986) 89.

[25] BRAMBILLA, M., CARDINALI, A., Plasma Physics 24 (1982) 1187.

[26] BHATNAGAR, V., KOCH, R., GEILFUS, P., et al., Nucl. Fusion 24 (1984) 955.

[27] HWANG, D.Q., KARNEY, C.F.F., HOSEA, J.C., et al., Modeling of ICRF Heating of a Tokamak Plasma, report PPPL-1990, Princeton Plasma Phys. Lab. (1983).

[28] PHILLIPS, C. K., PERKINS, F.W., HWANG, D.Q., Phys. Fluids 29 (1986) 1608.

[29] COLESTOCK, P. L., KASHUBA, R. J., Nucl. Fusion 23 (1983) 763.

[30] FUKUYAMA, A., GOTO, A., ITOH, S.-I., ITOH, K., Jap. J. Appl. Phys. Lett. 23 (1984) 613.

[31] VILLARD, L., APPERT, K., GRUBER, R., VACLAVIK,J., Comp. Phys. Rep. 4 (1986) 95.

[32] FUKUYAMA, A., ITOH, K., ITOH, S.-I., Comp. Phys. Rep. 4 (1986) 137.

[33] KRUECKEN, T., BRAMBILLA, M., in Controlled Fusion and Plasma Physics (Proc. 14th Europ. Conf. Madrid, 1987) Vol.11 D, Part II, EPS (1987) 996.

[34] ITOH, S.-I., FUKUYAMA, A., ITOH, K., Nucl. Fusion 24 (1984) 224.

[35] SOELL, M., WESNER, F., in Fusion Engineering (Proc. 10th Symp. Philadelphia, 1983) Vol.1 (1983) 600.

[36] NOTERDAEME, J.-M., RYTER, F., SOELL, M., et al., in Controlled Fusion and Plasma Heating (Proc. 13th Europ. Conf. Schliersee, 1986) Vol.10 C, Part II, EPS (1986) 137.

[37] WESNER, F., BRAUN, F., FRITSCH, R., et al., in Heating in Toroidal Plasmas (Proc. 3rd Joint Varenna-Grenoble Intern. Symp. Grenoble) Vol. 1, CEC (1982) 429.

[38] WESNER, F., BRAUN, F., FRITSCH, R., et al., in Heating in Toroidal Plasmas (Proc. 4th Intern. Symp. Rome, 1984) Vol.II (1984) 1103.

[39] STEINMETZ, K., WESNER, F., NIEDERMEYER, H., et al., J. Vac. Sci. Technol. A4 (3), (1986) 1088.

[40] STEINMETZ, K., in Applications of Radio-Frequency Power to Plasmas (Proc. 7th Topical Conf. Kissimmee) APS (1987) 211.

[41] STEINMETZ, K., FUSSMANN, G., GRUBER, O., et al., Plasma Physics and Controlled Nucl. Fusion 28 (1986) 235.

[42] STEINMETZ, K., WAGNER, F., WESNER, F., et al., in Controlled Fusion and Plasma Heating (Proc. 13th Europ. Conf. Schliersee, 1986) Vol.10 C, Part II, EPS (1986) 21.

[43] STEINMETZ, K., SOELDNER, F.X., ECKHARTT, D., et al., in Plasma Physics and Controlled Nuclear Fusion Research (Proc. 11th Conf. Kyoto, 1986) Vol.1, IAEA, Vienna (1987) 461.

[44] BEHRINGER, K.H., DENNE, B., FORREST, M.J., et al., in Controlled Fusion and Plasma Heating (Proc. 13th Europ. Conf. Schliersee, 1986) Vol.10 C, Part I, EPS (1986) 176.

[45] ITOH, S.-I., ITOH, K., FUKUYAMA, A., et al., ICRF Heating Analysis on ASDEX Plasmas, report IPP III /115, Max-Planck-Institut fuer Plasmaphysik, Garching (1987).

[46] ADAM, J., equipe TFR, Plasma Physics and Controlled Fusion 26 (1984) 165.

[47] MATSUMOTO, H., private communication.

[48] ONO, M., BEIERSDORFER, P., BELL, R., et al., in Plasma Physics and Controlled Nuclear Fusion Research (Proc. 11th Intern. Conf. Kyoto, 1986) Vol. 1, IAEA, Vienna (1987) 477.

[49] JANESCHITZ, G., FUSSMANN, G., NOTERDAEME, J.-M., et al., in Controlled Fusion and Plasma Heating (Proc. 13th Europ. Conf. Schliersee, 1986) Vol.10 C, Part I, EPS (1986) 407.

[50] FUSSMANN, G., BARTIROMO, R., JANESCHITZ, G., et al., in Controlled Fusion and Plasma Physics (Proc. 12th Europ. Conf. Budapest, 1985), Vol. 9F, Part I, EPS (1985) 195.

[51] WAGNER, F., SOELDNER, F.X., STEINMETZ, K., et al., Plasma Physics and Controlled Fusion 28 (1986) 1225.

[52] RYTER, F., BROCKEN, H., IZVOZCHIKOV, A., et al., in Controlled Fusion and Plasma Heating (Proc. 13th Conf. Schliersee, 1986) Vol.10 C, Part I, EPS (1986) 101.

[53] ITOH, S.-I., ITOH, K., FUKUYAMA, A., Plasma Physics and Contr. Fusion 26 (1984) 1311.

[54] BRAMBILLA, M., STEINMETZ, K., in Heating in Toroidal Plasmas (Proc. 4th Intern. Symp. Rome, 1984) Vol.1 (1984) 351.

[55] STAEBLER, A., WAGNER, F., BECKER, G., et al., ibid, 3.

[56] STEINMETZ, K., BRAMBILLA, M., EBERHAGEN, A., et al., in Controlled Fusion and Plasma Physics (Proc. 14th Europ. Conf. Madrid, 1987) Vol.11 D, Part III, EPS (1987) 946.

[57] KEILHACKER, M., GIERKE, G.v., MUELLER, E.R., et al., Plasma Physics and Controlled Fusion 28 (1986) 29.

[58] LALLIA, P.P., JET team, Plasma Physics and Controlled Fusion 28 (1986) 1211.

[59] WAGNER, F., BARTIROMO, R., BECKER, G., et al., Nucl. Fusion 25 (1985) 1490.

[60] STEINMETZ, K., NOTERDAEME, J.-M., WAGNER, F., et al., Phys. Rev. Letters 58 (1987) 124.

[61] WEDLER, H., WESNER, F., SOELL, M., et al., in Fusion Technology (Proc. 14th Symp. Avignon, 1986) Vol.1 (1986) 715.

[62] MATSUMOTO, H., HASEGAWA, M., HOSHINO, K., et al., in Controlled Fusion and Plasma Physics (Proc. 14th Europ. Conf. Madrid, 1987) Vol.11 D, Part I, EPS (1987) 5.

[63] NOTERDAEME, J.-M., JANESCHITZ, G., McCORMICK, K., et al., ibid, Part II (1987) 678.

[64] MERTENS, V., KAUFMANN, M., BUECHL, K., et al., ibid, Part I (1987) 33.

[65] ADAM, J., Plasma Physics and Controlled Fusion 29 (1987) 443.

FIGURE CAPTIONS

Fig. 1 : Poloidal cross-section of ASDEX with ICRH antenna.

Fig. 2 : Averaged RF power density in at the antenne surface.

Fig. 3 : a) CX - energy spectra of $2\Omega_{CH}$

b) CX - energy spectra of D(H).

Fig. 4 : Summary plot of $\alpha = f (P_{IC}, P_{NI})$

β-rise, β-decrease and β-fit indicate the determination of α in the additional heating phase (NI or ICRH), at termination of heating or by the fit-procedure as described in the text.

Fig. 5 : Radiation power density profiles of ICRH under different wall conditions.

Fig. 6 : Variation of the global radiation level and edge localized fast ion fluxes with the resonance layer position.

Fig. 7 : Pure ICRF heated discharge (n_e, W_p, T_e, P_{IC}).

Fig. 8 : Heating efficiencies of $2\Omega_{CH}$ vs n_H/n_e.

Fig. 9 : Heating efficiencies vs P_{NI}.

Fig. 10 : a) direct electron heating efficiencies

b) ion heating efficiencies.

Fig. 11 : Normalized heating rates (the JET data represent the non-monster regime).

Fig. 12 : Energy confinement for D(H) and $2\Omega_{CH}$.

Fig. 13 : τ_E - summary.

Fig. 14 : W_p vs P_{tot} scaling of both RF regimes.

Fig. 15 : NI and subsequent ICRH in comparison.

Fig. 16 : TiXX-transport times vs power.

Fig. 17 : a) τ_E vs I_p (NI + ICRH)

b) τ_E vs n_e ($2\Omega_{CH}$).

Fig. 18 : a) NI + ICRH (n_e, W_p, T_e) vs time

b) T_{io} (NI+ICRH) vs time.

Fig. 19 : Pure D(H) heating achieving an H-phase marginally and temporal development of the T_e profile prior and after an H-transition.

Fig. 20 : Power dependent development of the H-mode with minority heating (B_o = 2.24 T, I_p = 320 kA).

Fig. 21 : RF antenna response to an H-transition.

Fig. 22 : $T_e(r)$ vs ICRH power.

Fig. 23 : Normalized T_e profiles of OH, NI, ICRH.

Fig. 24 : T_e and p_e profiles comparing NI and NI+ICRH at equal total heating power.

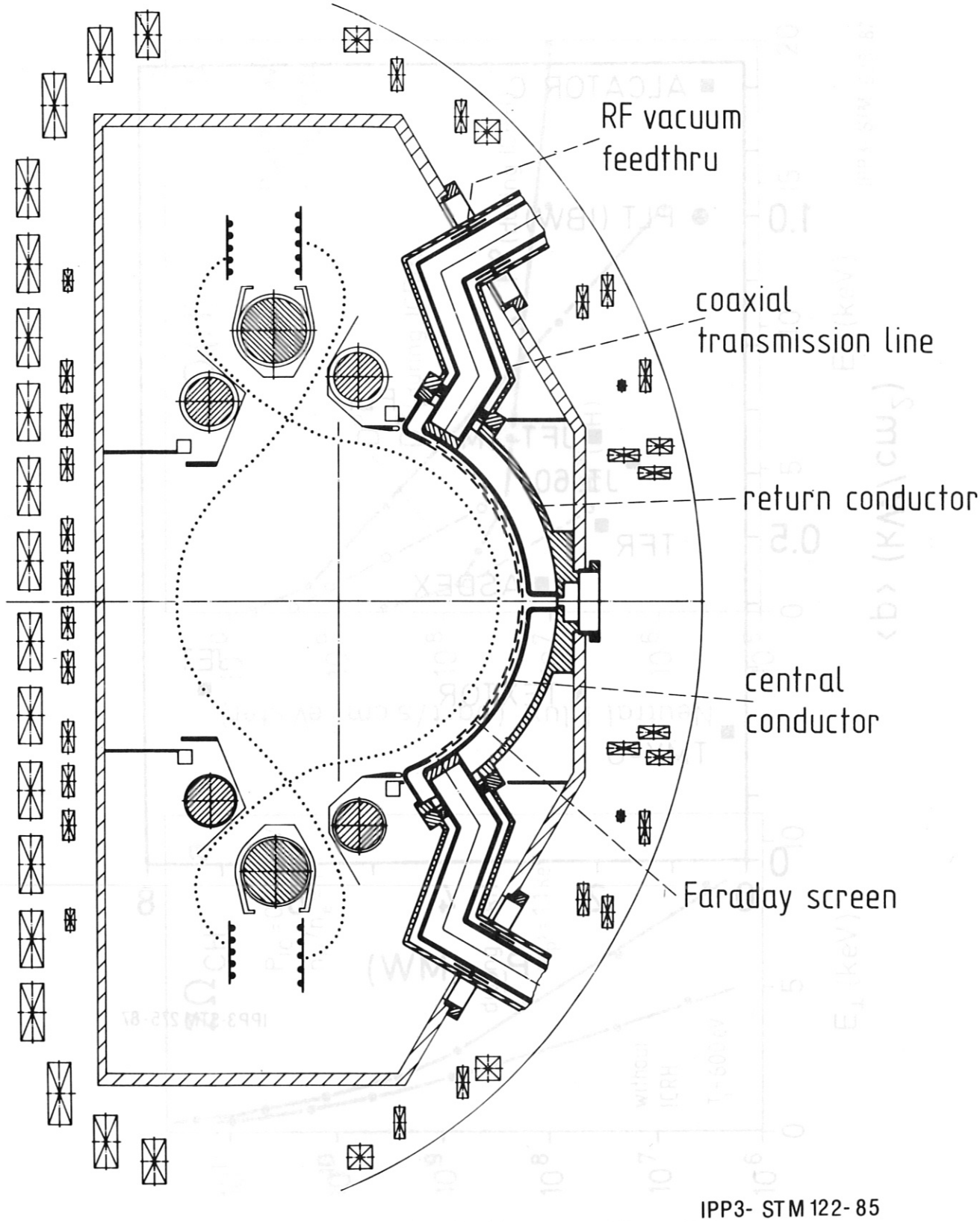
RF vacuum
feedthru
coaxial
transmission line
return conductor
central
conductor
Faraday screen
IPP3- STM 122-85

Fig. 1

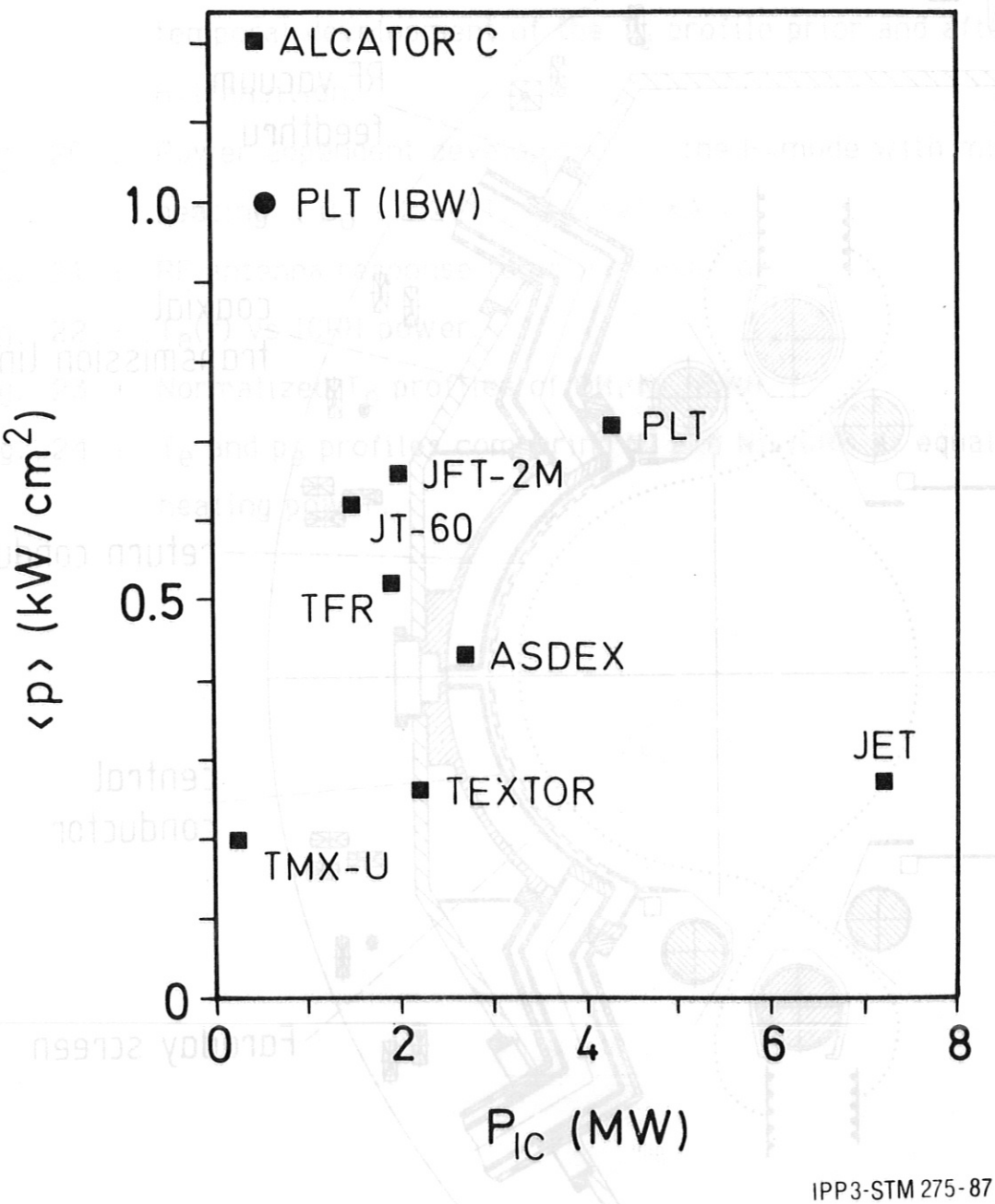
ALCATOR C
PLT (IBW)
PLT
JFT-2M
JT-60
TFR
ASDEX
JET
TEXTOR
TMX-U
1.0
0.5
0
0
2
4
6
8
<p> (kW/cm²)
P_IC (MW)
IPP3-STM 275-87

Fig. 2

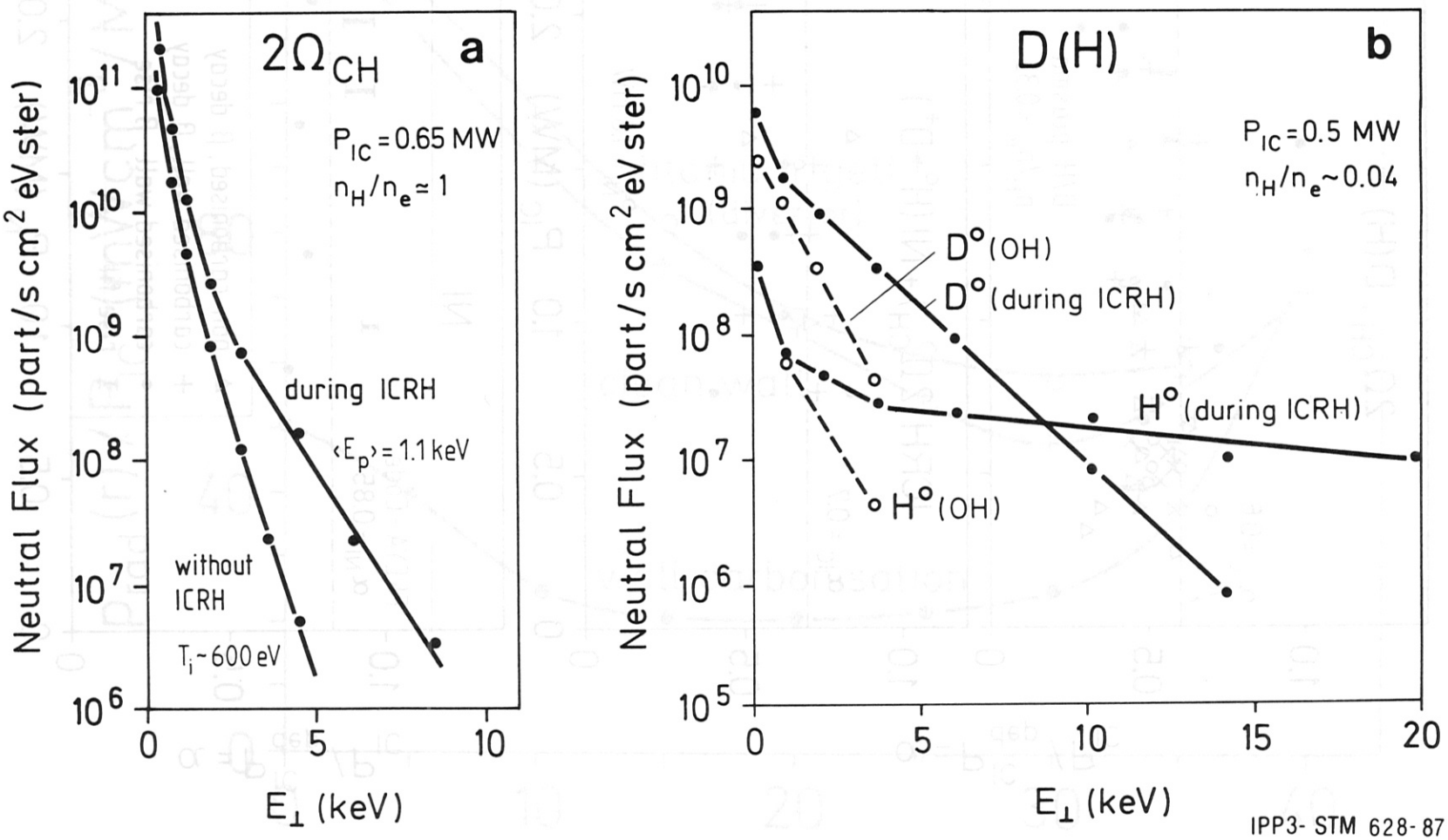
2Ω CH
a
P_IC = 0.65 MW
n_H/n_e ≃ 1
during ICRH
⟨E_p⟩ = 1.1 keV
without ICRH
T_i ~ 600 eV
Neutral Flux (part/s cm² eV ster)
E⊥ (keV)
D (H)
b
P_IC = 0.5 MW
n_H/n_e ~ 0.04
D° (OH)
D° (during ICRH)
H° (during ICRH)
H° (OH)
IPP3- STM 628-87

Fig. 3

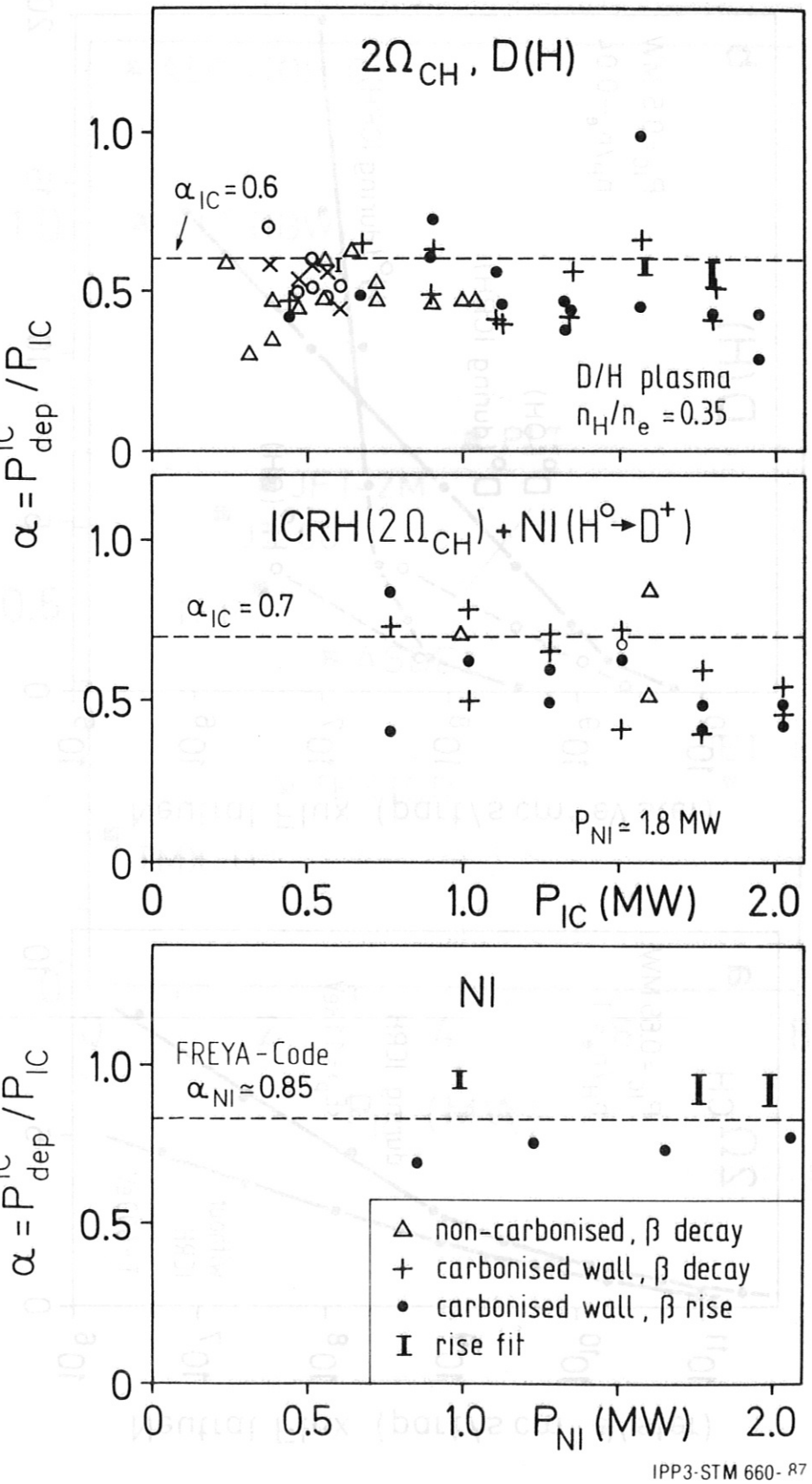
2Ω CH , D(H)
α IC = 0.6
D/H plasma
n H/n e = 0.35
ICRH(2Ω CH) + NI (H°→D+)
α IC = 0.7
P NI ≈ 1.8 MW
NI
FREYA - Code
α NI ≈ 0.85
△ non-carbonised, β decay
+ carbonised wall, β decay
• carbonised wall, β rise
I rise fit
α = P dep IC / P IC
P IC (MW)
P NI (MW)
0
0.5
1.0
2.0
IPP3-STM 660- 87

Fig. 4

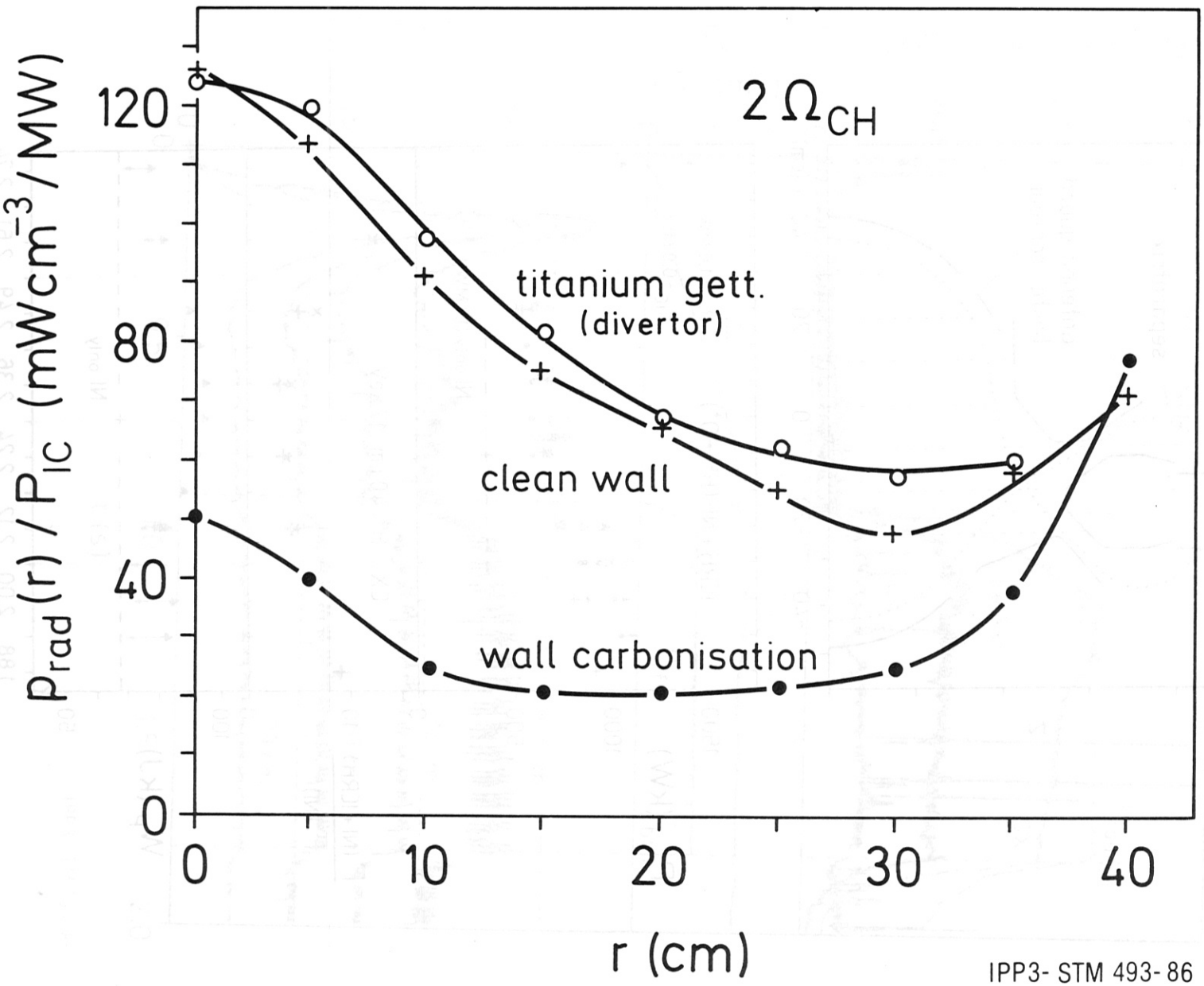

IPP3- STM 493- 86

Fig. 5

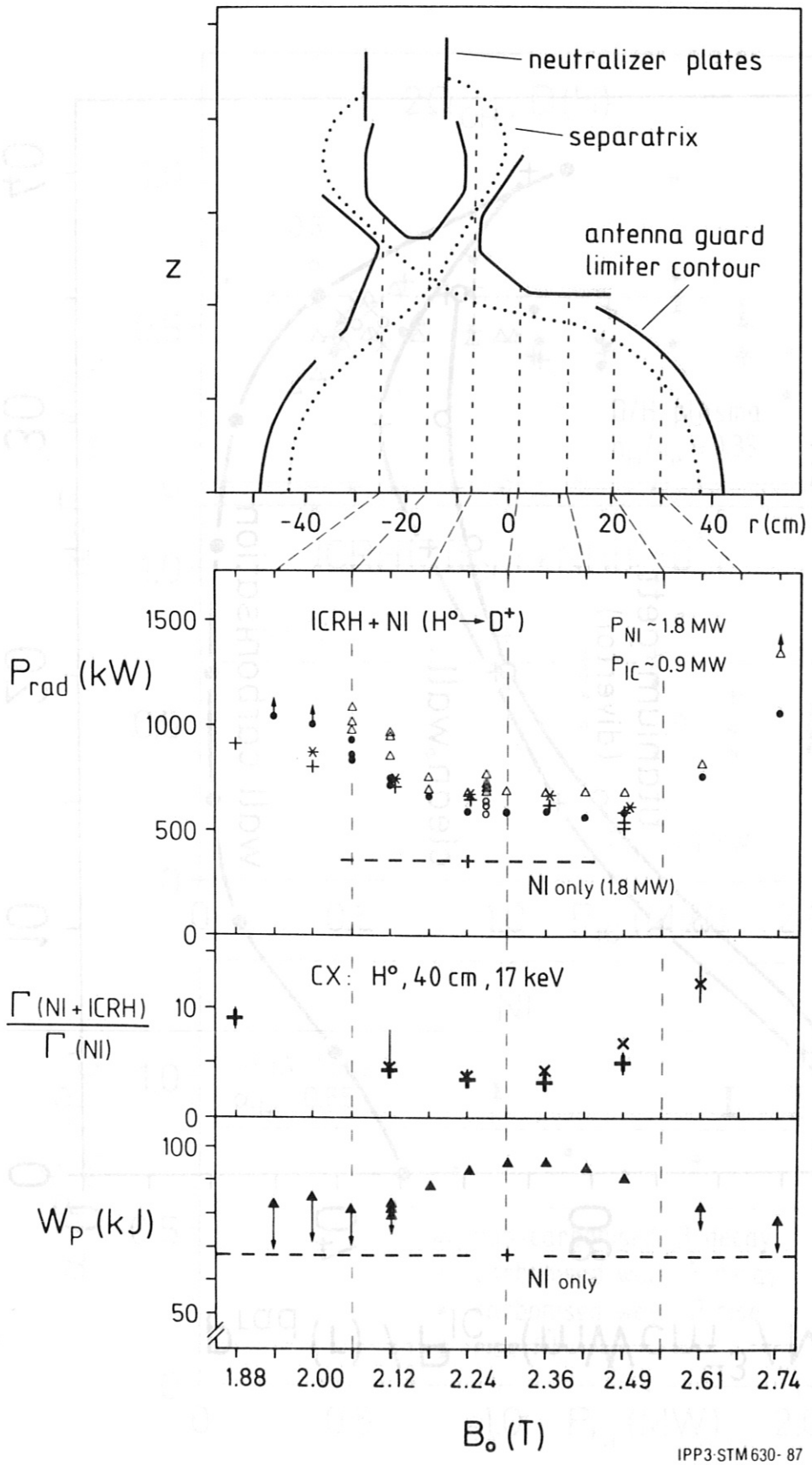
neutralizer plates
separatrix
antenna guard
limiter contour
z
-40
-20
0
20
40
r (cm)
ICRH + NI (H°→D⁺)
P_NI ~ 1.8 MW
P_IC ~ 0.9 MW
P_rad (kW)
1500
1000
500
0
NI only (1.8 MW)
CX: H°, 40 cm, 17 keV
Γ (NI + ICRH) / Γ (NI)
10
0
100
W_p (kJ)
NI only
50
1.88
2.00
2.12
2.24
2.36
2.49
2.61
2.74
B_o (T)
IPP3-STM 630-87

Fig. 6

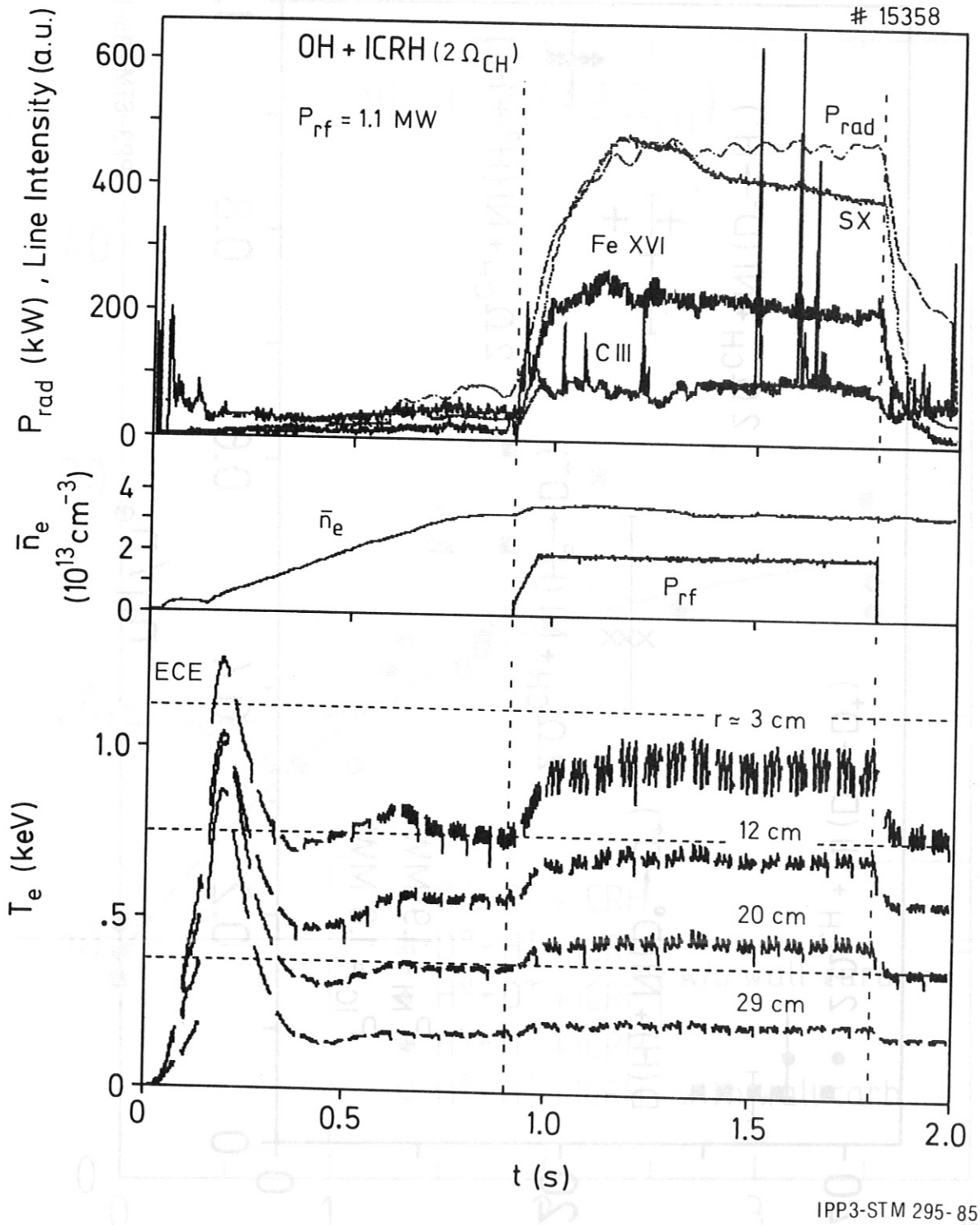
15358
OH + ICRH (2 Ω_CH)
P_rf = 1.1 MW
P_rad
SX
Fe XVI
C III
P_rad (kW) , Line Intensity (a.u.)
600
400
200
0
n̄_e
n̄_e (10^13 cm^-3)
4
2
0
P_rf
ECE
r ≈ 3 cm
12 cm
20 cm
29 cm
T_e (keV)
1.0
.5
0
0
0.5
1.0
1.5
2.0
t (s)
IPP3-STM 295-85

Fig. 7

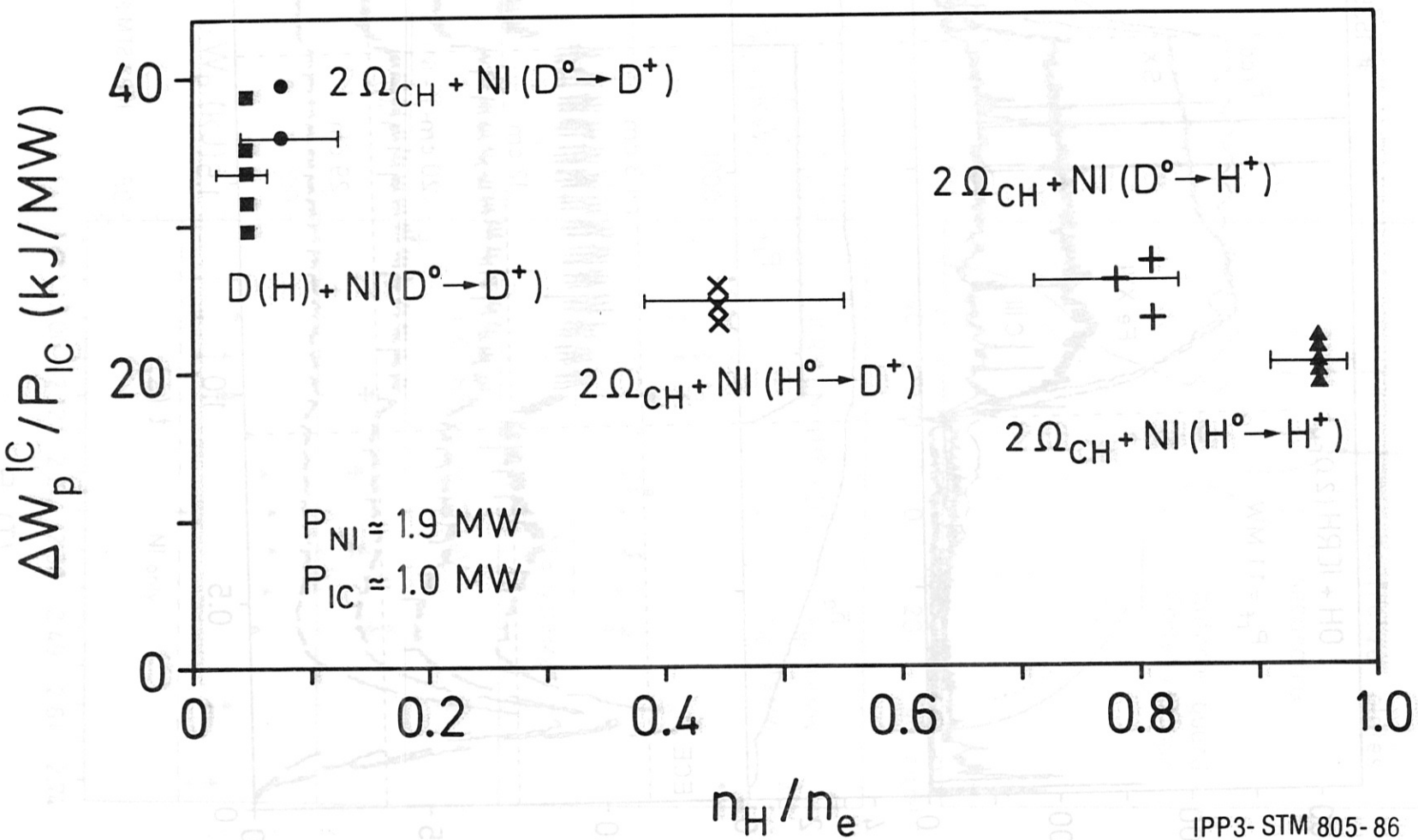
40
20
0
0
0.2
0.4
0.6
0.8
1.0
$\Delta W_p^{IC}/P_{IC}$ (kJ/MW)
n_H/n_e
$2\,\Omega_{CH}$ + NI ($D^\circ \rightarrow D^+$)
D(H) + NI($D^\circ \rightarrow D^+$)
$2\,\Omega_{CH}$ + NI ($H^\circ \rightarrow D^+$)
$2\,\Omega_{CH}$ + NI ($D^\circ \rightarrow H^+$)
$2\,\Omega_{CH}$ + NI ($H^\circ \rightarrow H^+$)
$P_{NI} \simeq 1.9$ MW
$P_{IC} \simeq 1.0$ MW
IPP3- STM 805- 86

Fig. 8

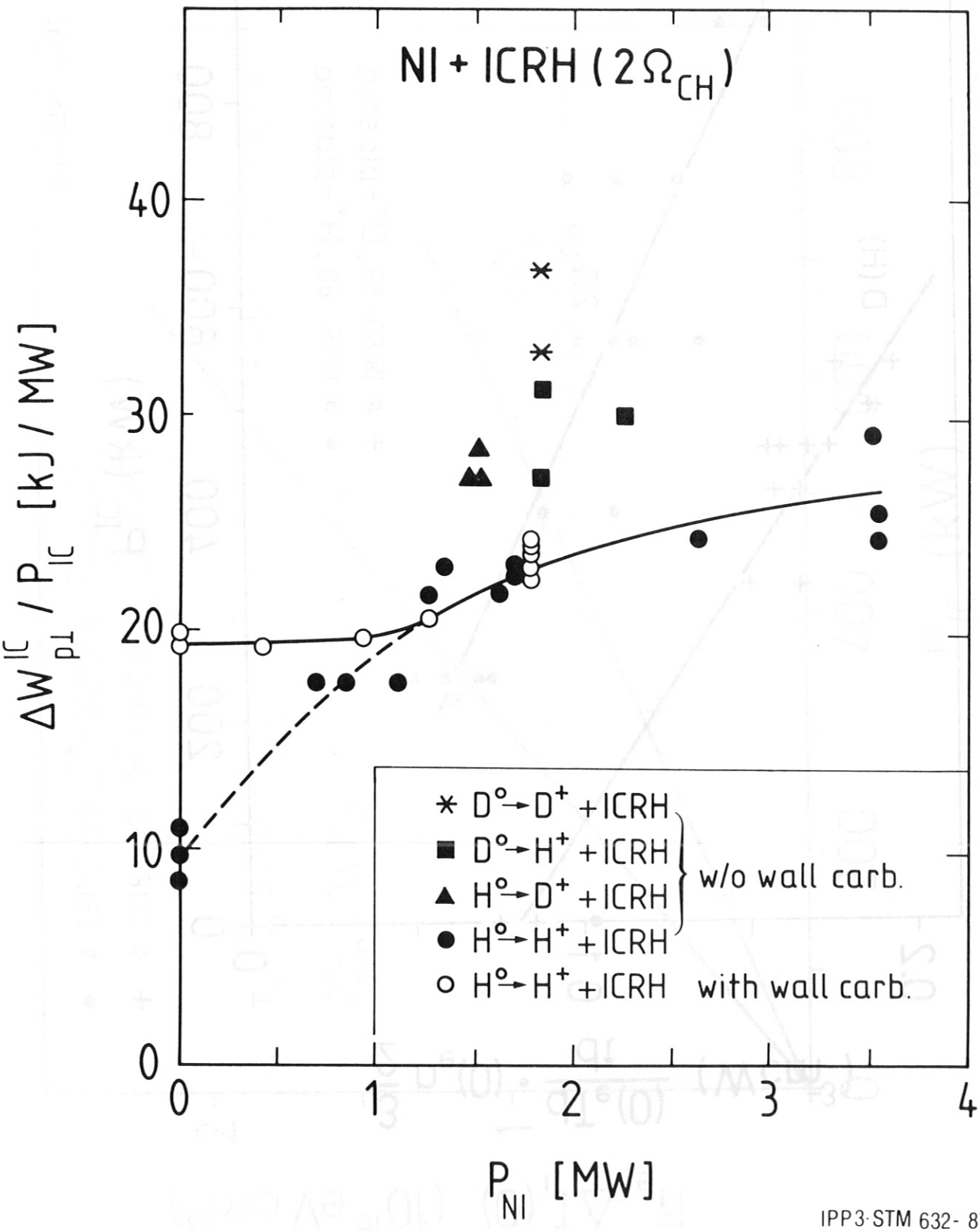

IPP3·STM 632- 87

Fig. 9

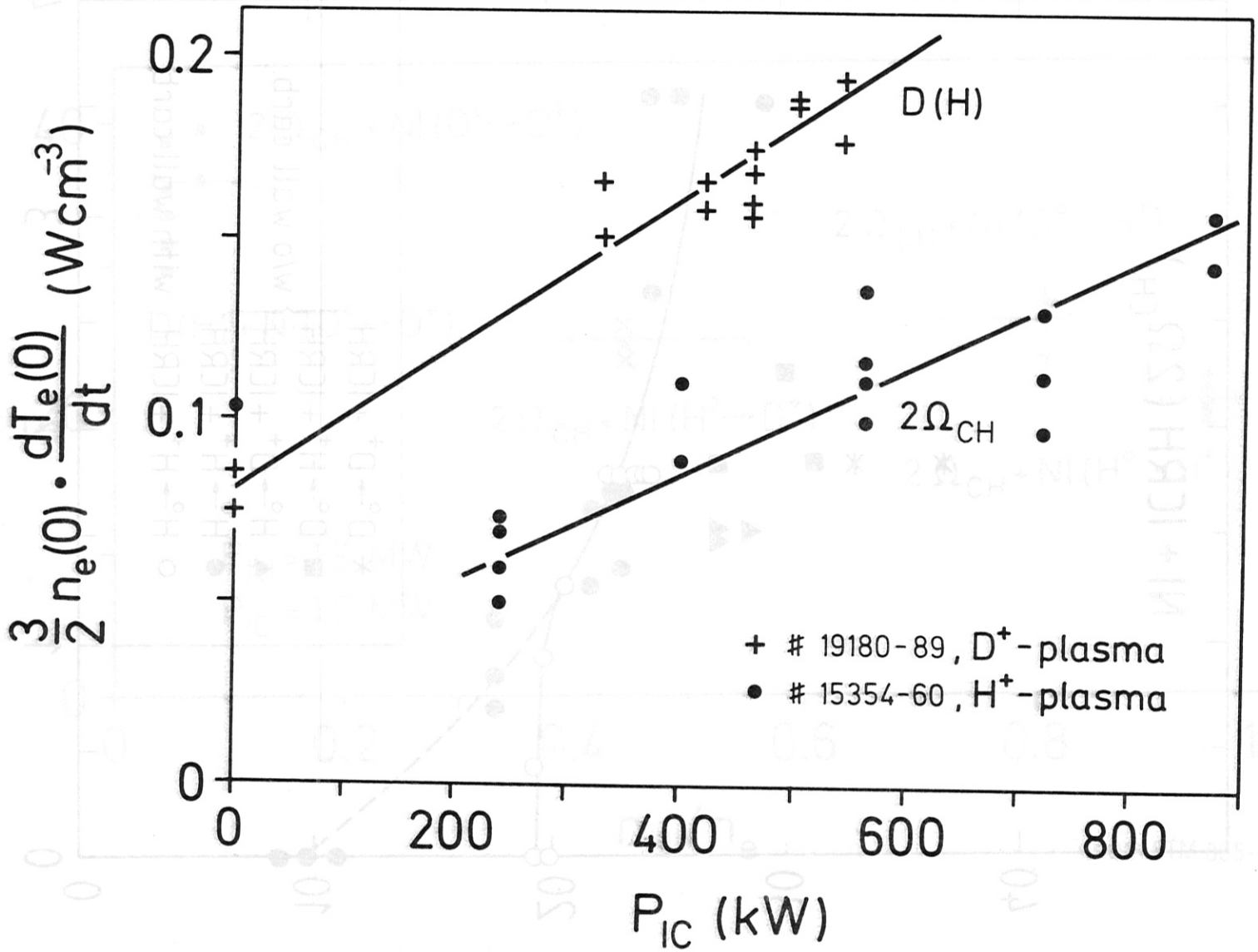

IPP3- STM 373-86

Fig. 10a

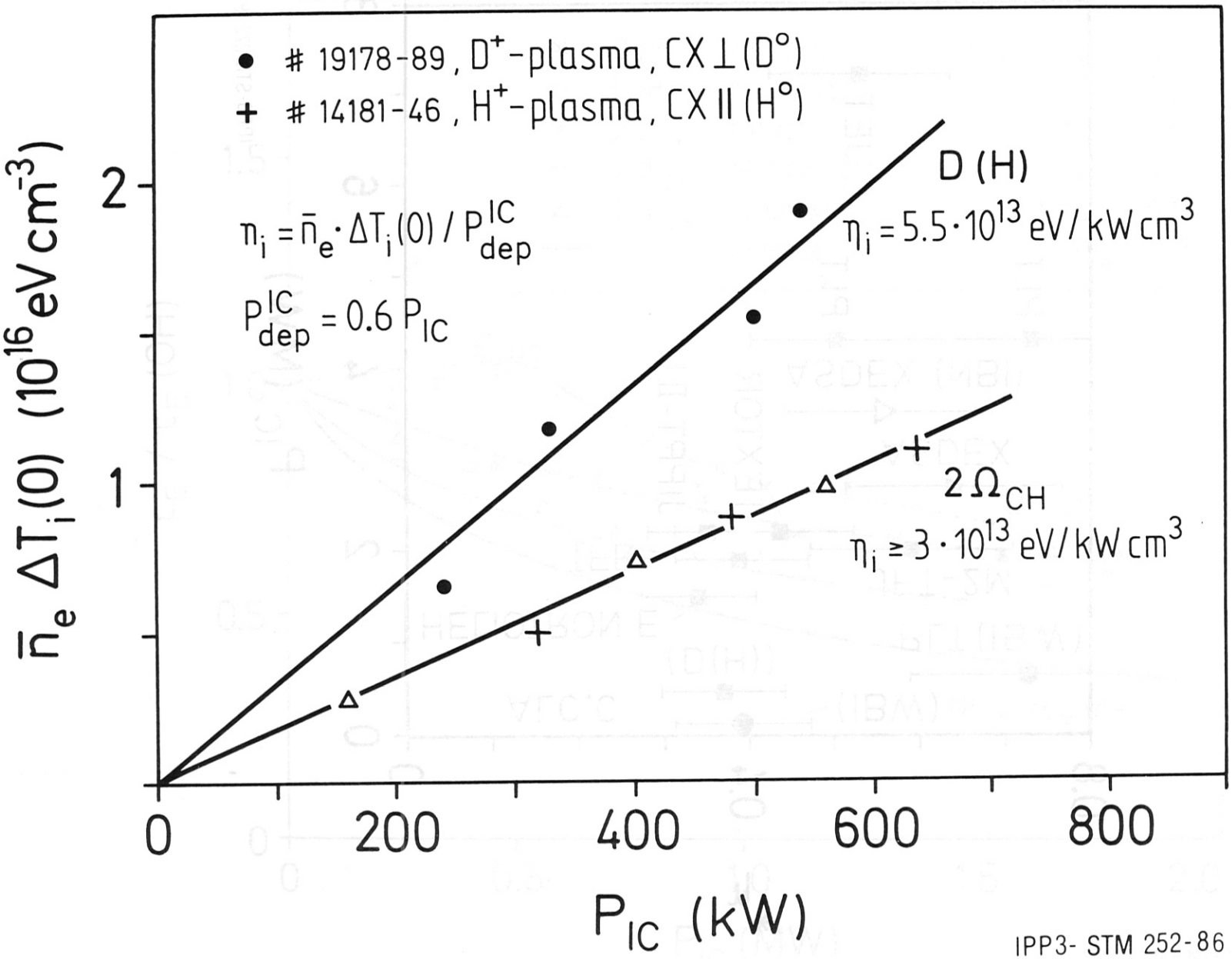
● # 19178-89 , D⁺-plasma , CX ⊥ (D°)
+ # 14181-46 , H⁺-plasma , CX ∥ (H°)
$\eta_i = \bar{n}_e \cdot \Delta T_i(0) / P_{dep}^{IC}$
$P_{dep}^{IC} = 0.6\, P_{IC}$
D (H)
$\eta_i = 5.5 \cdot 10^{13}$ eV / kW cm³
$2\Omega_{CH}$
$\eta_i \geq 3 \cdot 10^{13}$ eV / kW cm³
$\bar{n}_e\, \Delta T_i(0)$ $(10^{16}$ eV cm$^{-3})$
0
1
2
0
200
400
600
800
P_{IC} (kW)
IPP3- STM 252-86

Fig. 10b

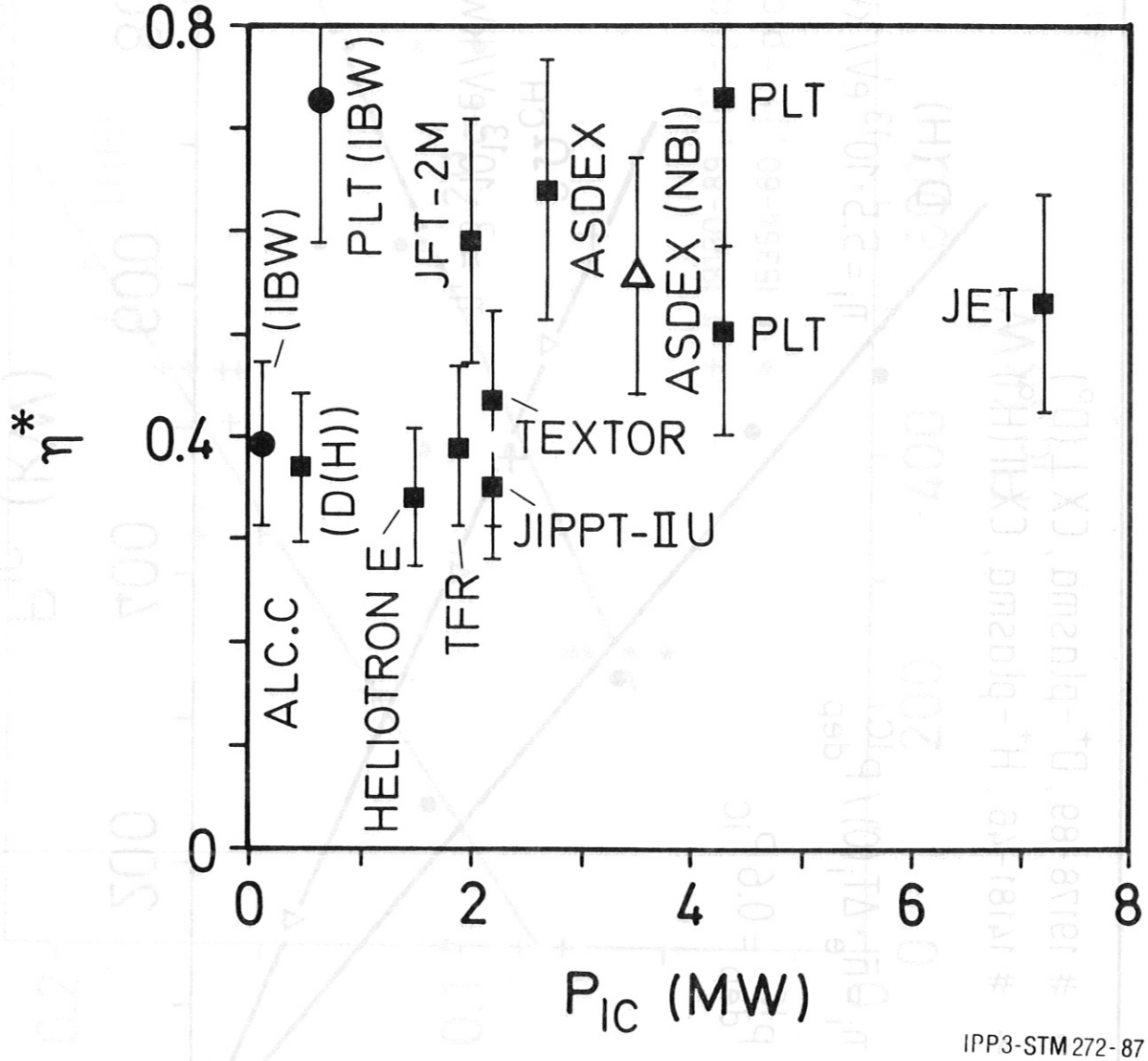
0.8
0.4
0
η^*
0
2
4
6
8
P_{IC} (MW)
(IBW)
(D(H))
ALC.C
PLT (IBW)
HELIOTRON E
JFT-2M
TFR
ASDEX
TEXTOR
JIPPT-IIU
ASDEX (NBI)
PLT
PLT
JET
IPP3-STM 272-87

Fig. 11

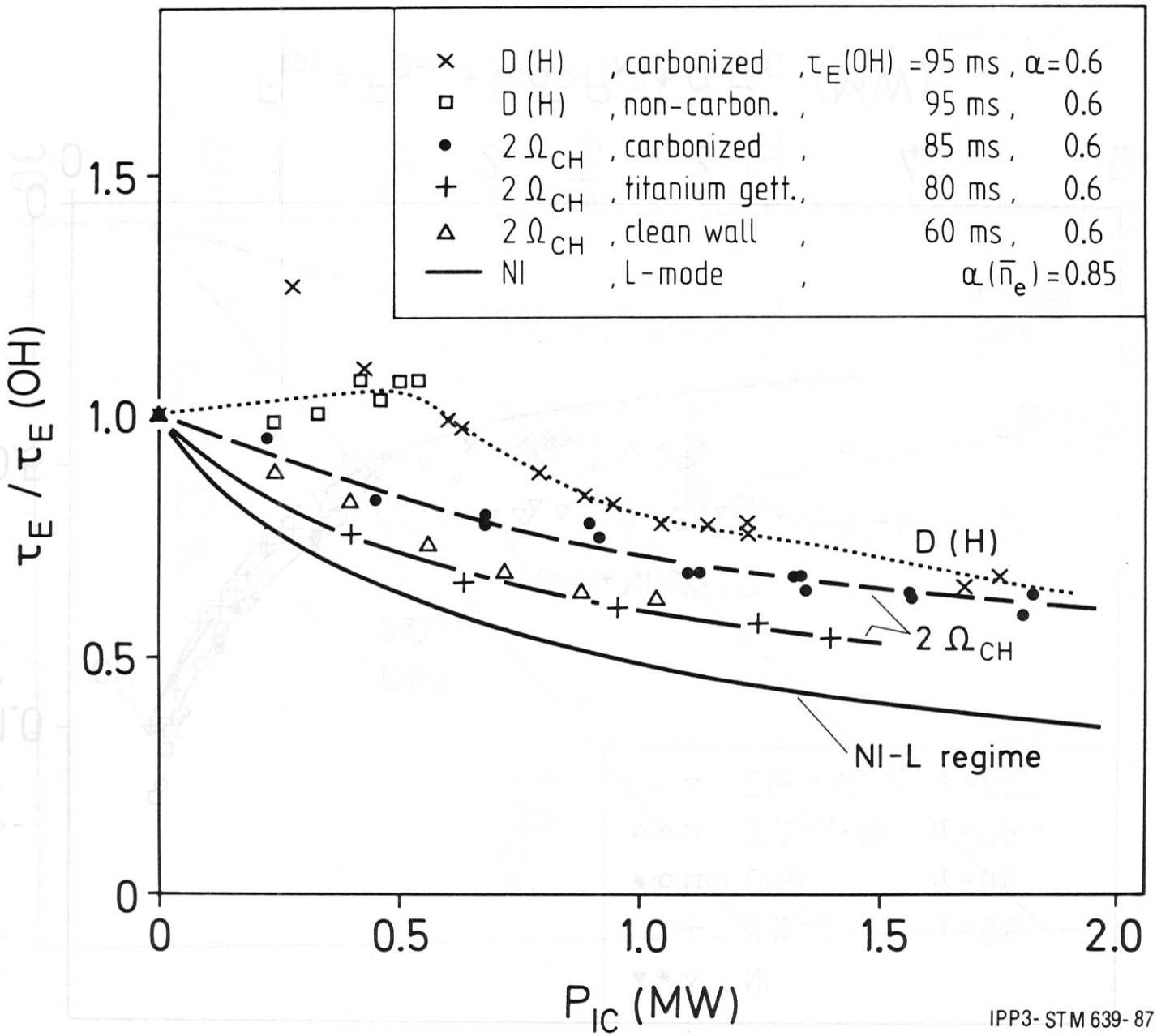
× D (H) , carbonized , τ_E(OH) = 95 ms , α = 0.6
□ D (H) , non-carbon. , 95 ms , 0.6
• 2 Ω_{CH} , carbonized , 85 ms , 0.6
+ 2 Ω_{CH} , titanium gett., 80 ms , 0.6
△ 2 Ω_{CH} , clean wall , 60 ms , 0.6
— NI , L-mode , α($\bar{n}_e$) = 0.85
D (H)
2 Ω_{CH}
NI-L regime
τ_E / τ_E(OH)
P_{IC} (MW)
0
0.5
1.0
1.5
2.0
IPP3-STM 639-87

Fig. 12

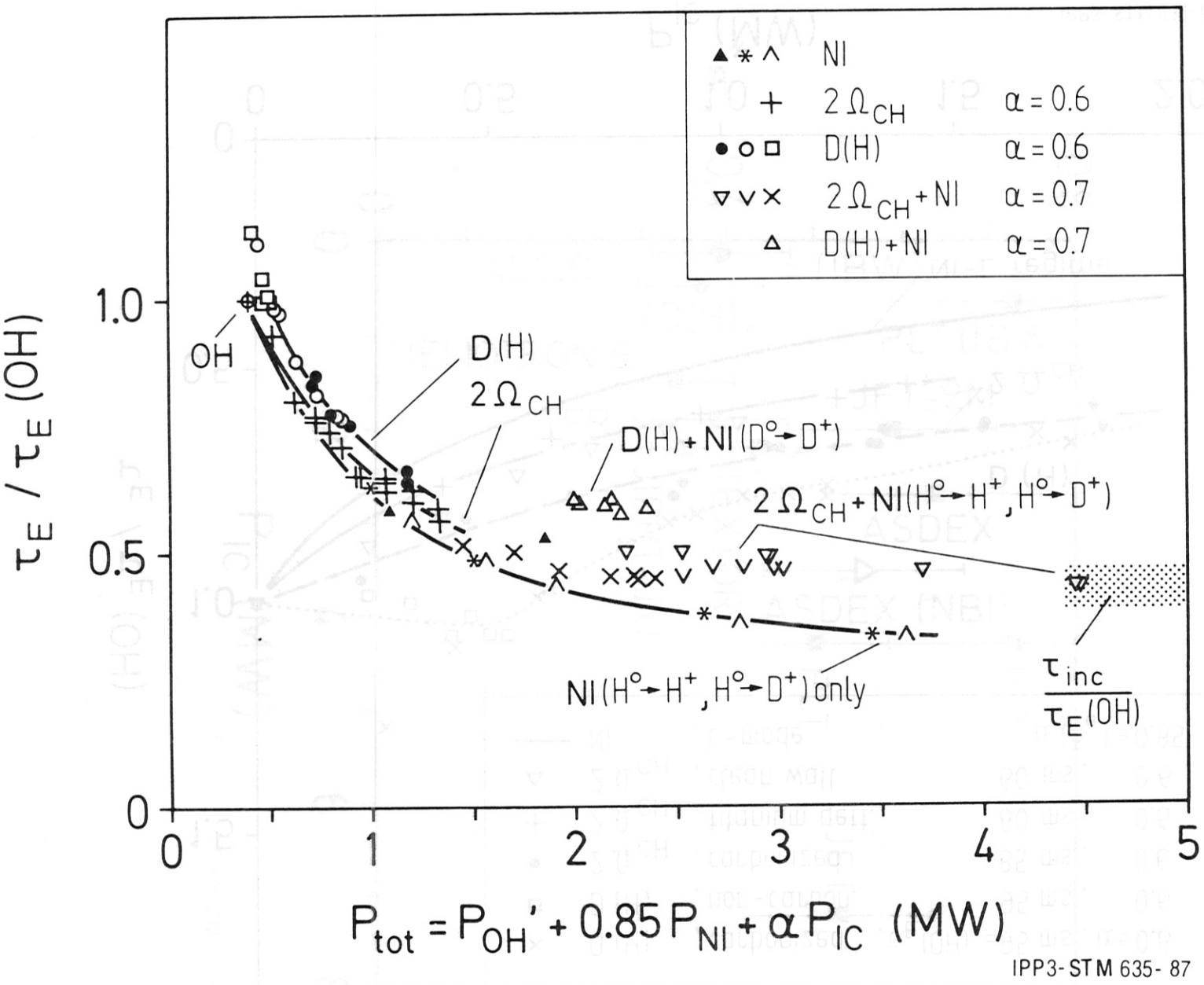
▲ * ^ NI
+ 2 Ω CH α = 0.6
● ○ □ D(H) α = 0.6
▽ v × 2 Ω CH + NI α = 0.7
△ D(H) + NI α = 0.7
τE / τE (OH)
1.0
0.5
0
OH
D(H)
2 Ω CH
D(H) + NI (D° → D+)
2 Ω CH + NI (H° → H+, H° → D+)
NI (H° → H+, H° → D+) only
τ inc / τE (OH)
0
1
2
3
4
5
Ptot = POH' + 0.85 PNI + α PIC (MW)
IPP3-STM 635-87

Fig. 13

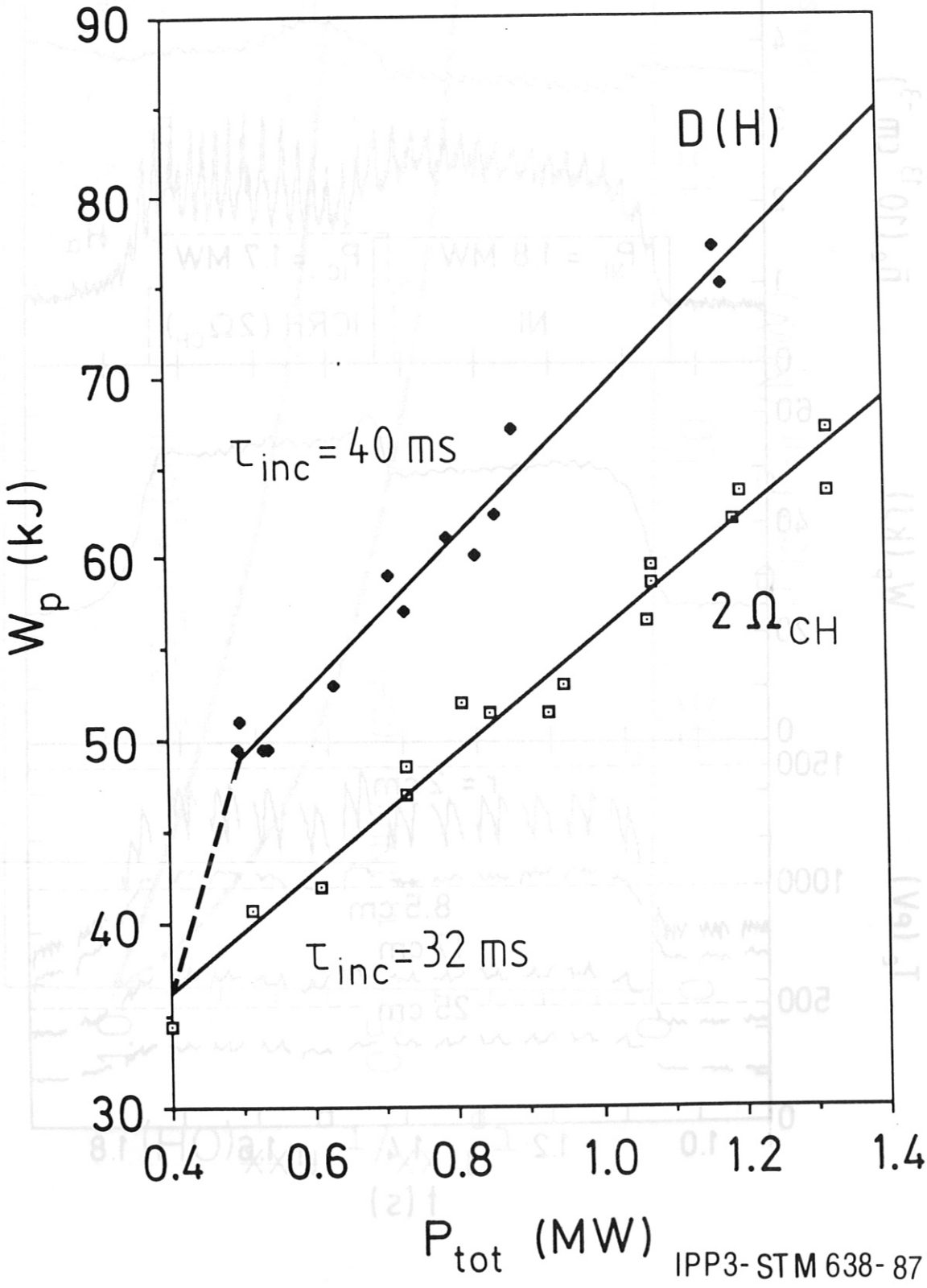
90
80
70
60
50
40
30
W_p (kJ)
D(H)
τ_{inc} = 40 ms
2 Ω_{CH}
τ_{inc} = 32 ms
0.4
0.6
0.8
1.0
1.2
1.4
P_{tot} (MW)
IPP3-STM 638-87

Fig. 14

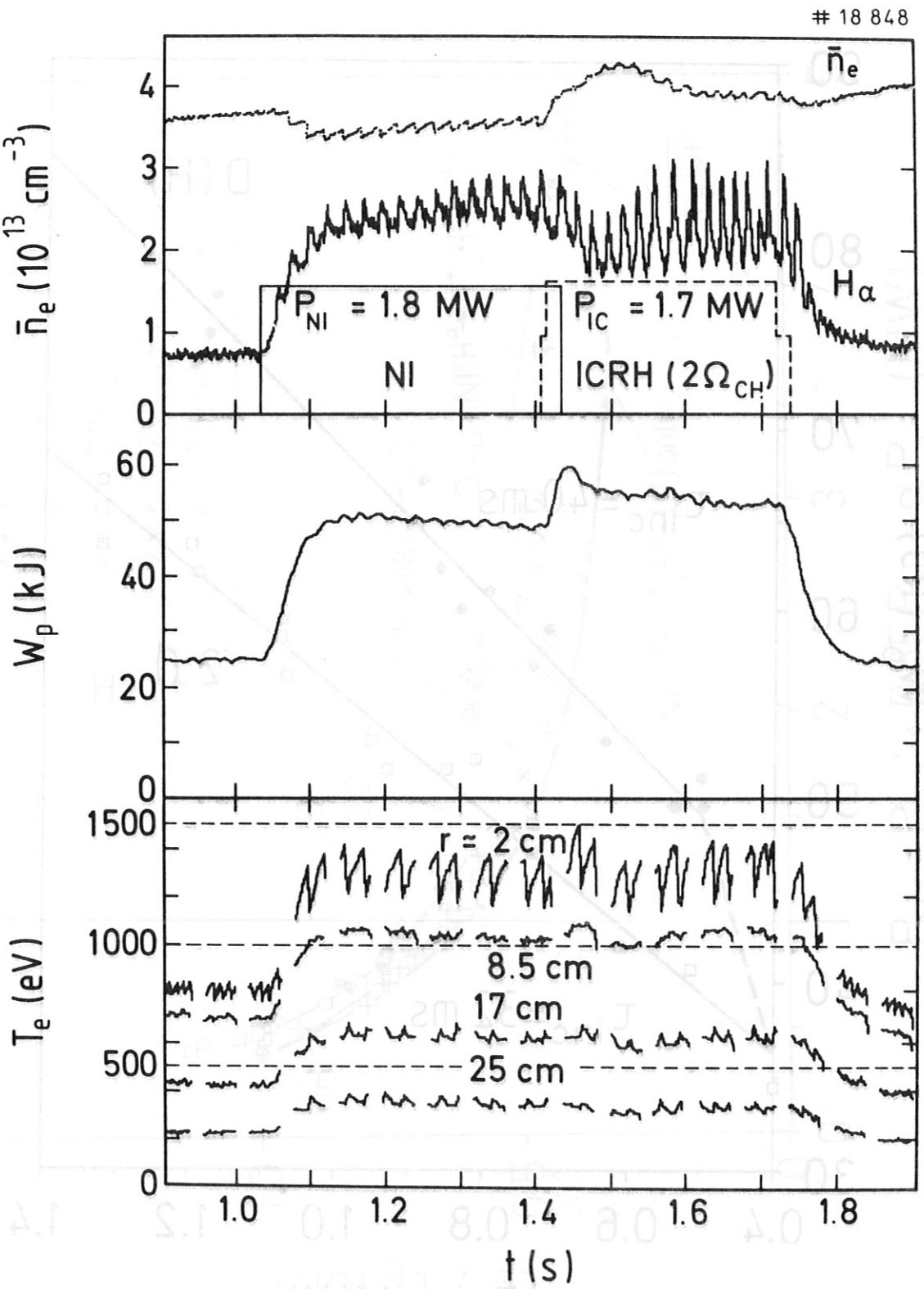
18 848
$\bar{n}_e$
$\bar{n}_e$ (10^{13} cm^{-3})
H_α
P_{NI} = 1.8 MW
NI
P_{IC} = 1.7 MW
ICRH ($2\Omega_{CH}$)
W_p (kJ)
T_e (eV)
r = 2 cm
8.5 cm
17 cm
25 cm
t (s)

Fig. 15

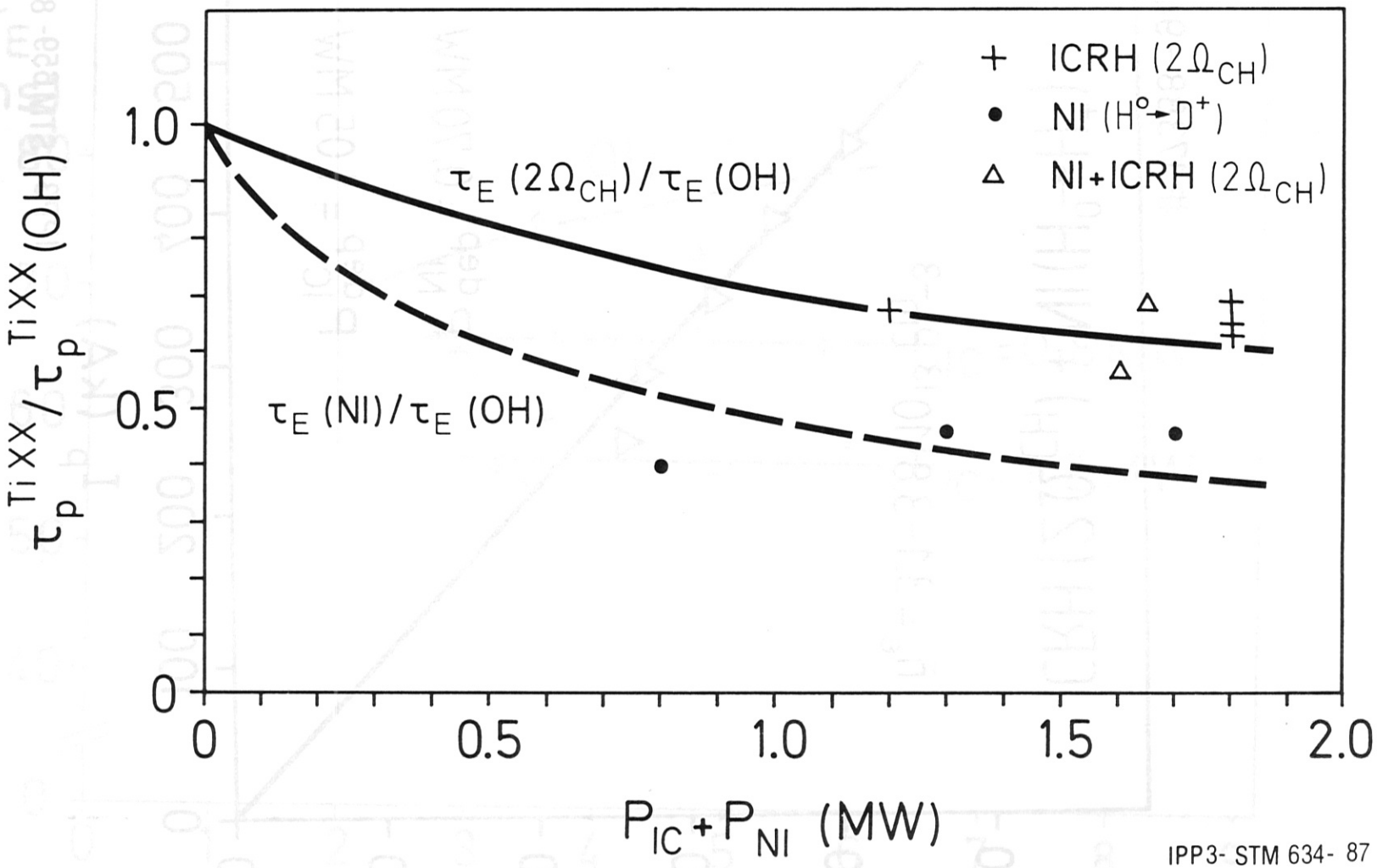
+ ICRH (2Ω_CH)
• NI (H°→D⁺)
△ NI+ICRH (2Ω_CH)
τ_E (2Ω_CH) / τ_E (OH)
τ_E (NI) / τ_E (OH)
τ_p^TiXX / τ_p^TiXX (OH)
1.0
0.5
0
0
0.5
1.0
1.5
2.0
P_IC + P_NI (MW)
IPP3- STM 634- 87

Fig. 16

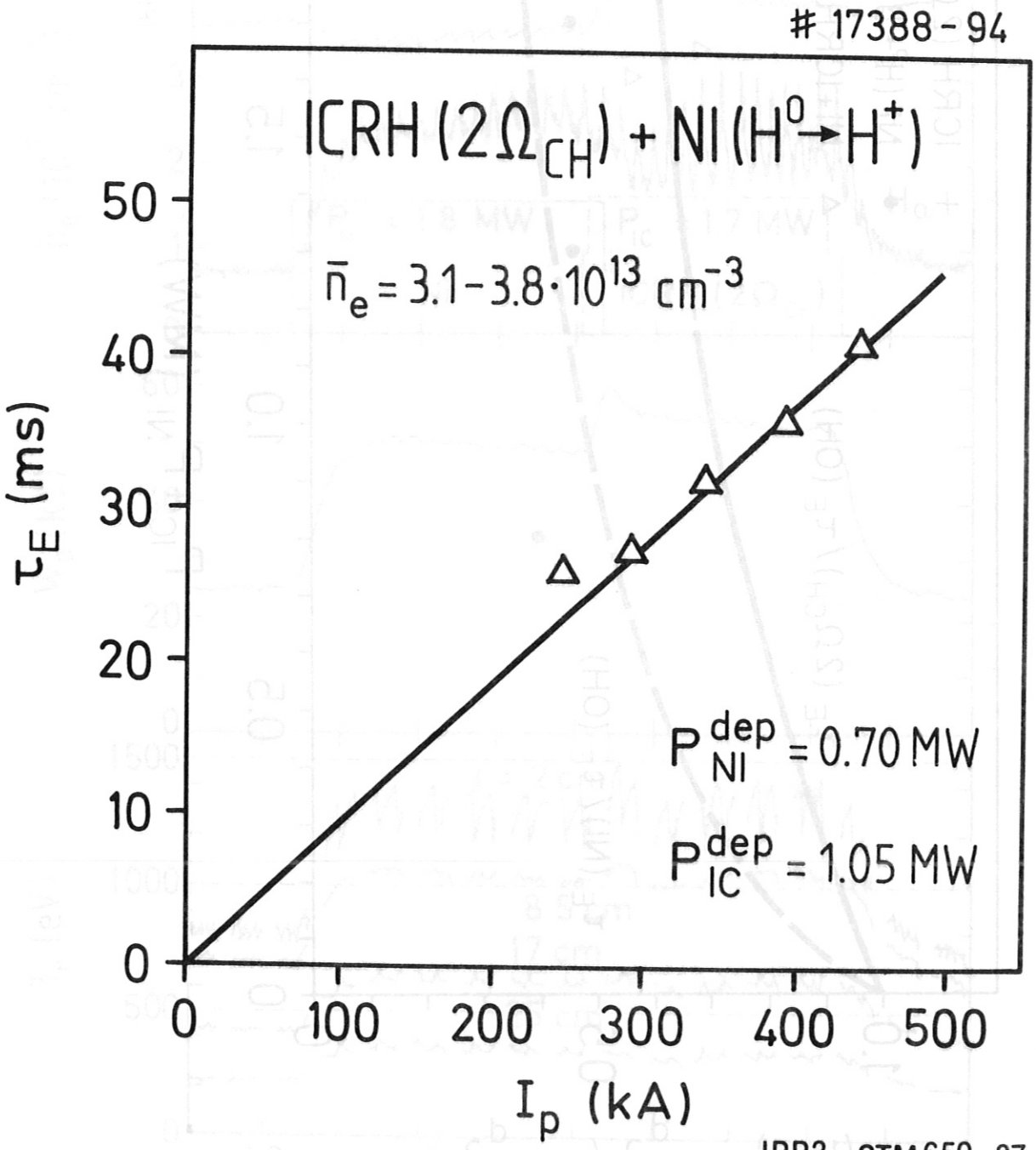
17388 - 94
ICRH ($2\Omega_{CH}$) + NI ($H^0 \rightarrow H^+$)
$\bar{n}_e = 3.1 - 3.8 \cdot 10^{13}$ cm^{-3}
$P_{NI}^{dep} = 0.70$ MW
$P_{IC}^{dep} = 1.05$ MW
τ_E (ms)
I_p (kA)
0
10
20
30
40
50
0
100
200
300
400
500
IPP3- STM 659- 87

Fig. 17a

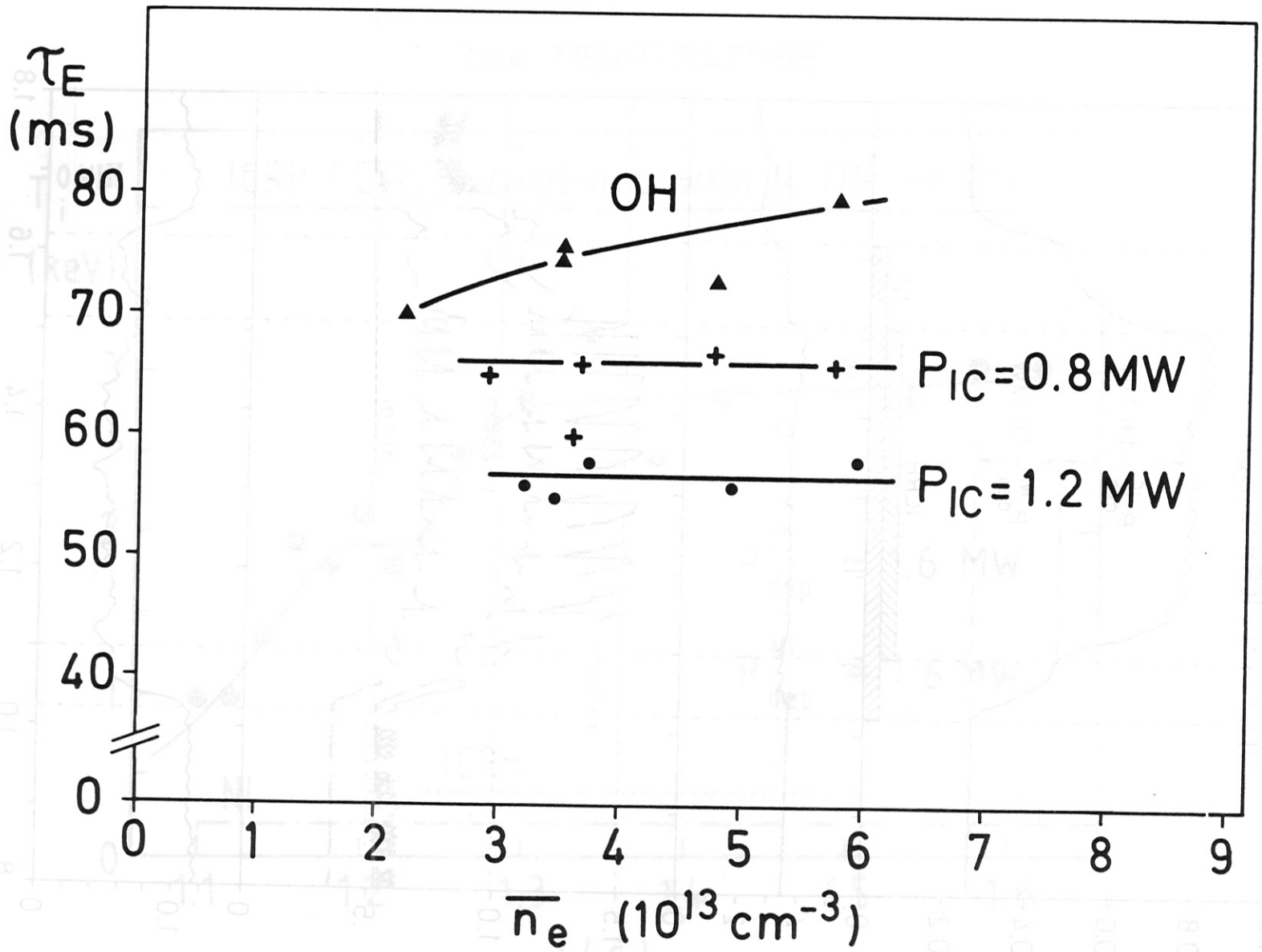

IPP3- STM 631- 87

Fig. 17b

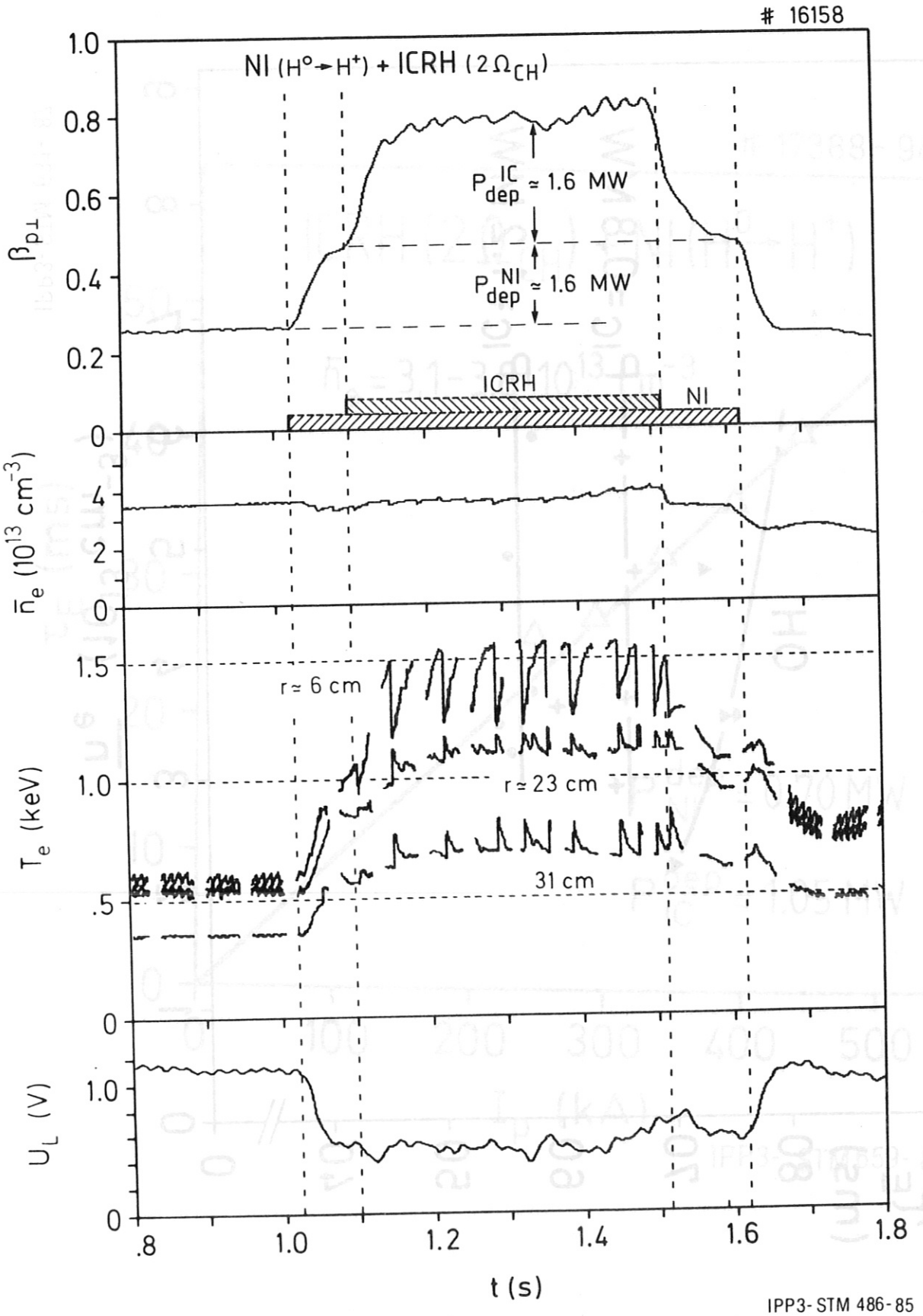
16158
NI (H°→H⁺) + ICRH (2Ω_CH)
β_pt
P_dep^IC ≈ 1.6 MW
P_dep^NI ≈ 1.6 MW
ICRH
NI
n̄_e (10^13 cm^-3)
T_e (keV)
r ≈ 6 cm
r ≈ 23 cm
31 cm
U_L (V)
t (s)
IPP3-STM 486-85

Fig. 18a

ION TEMPERATURE

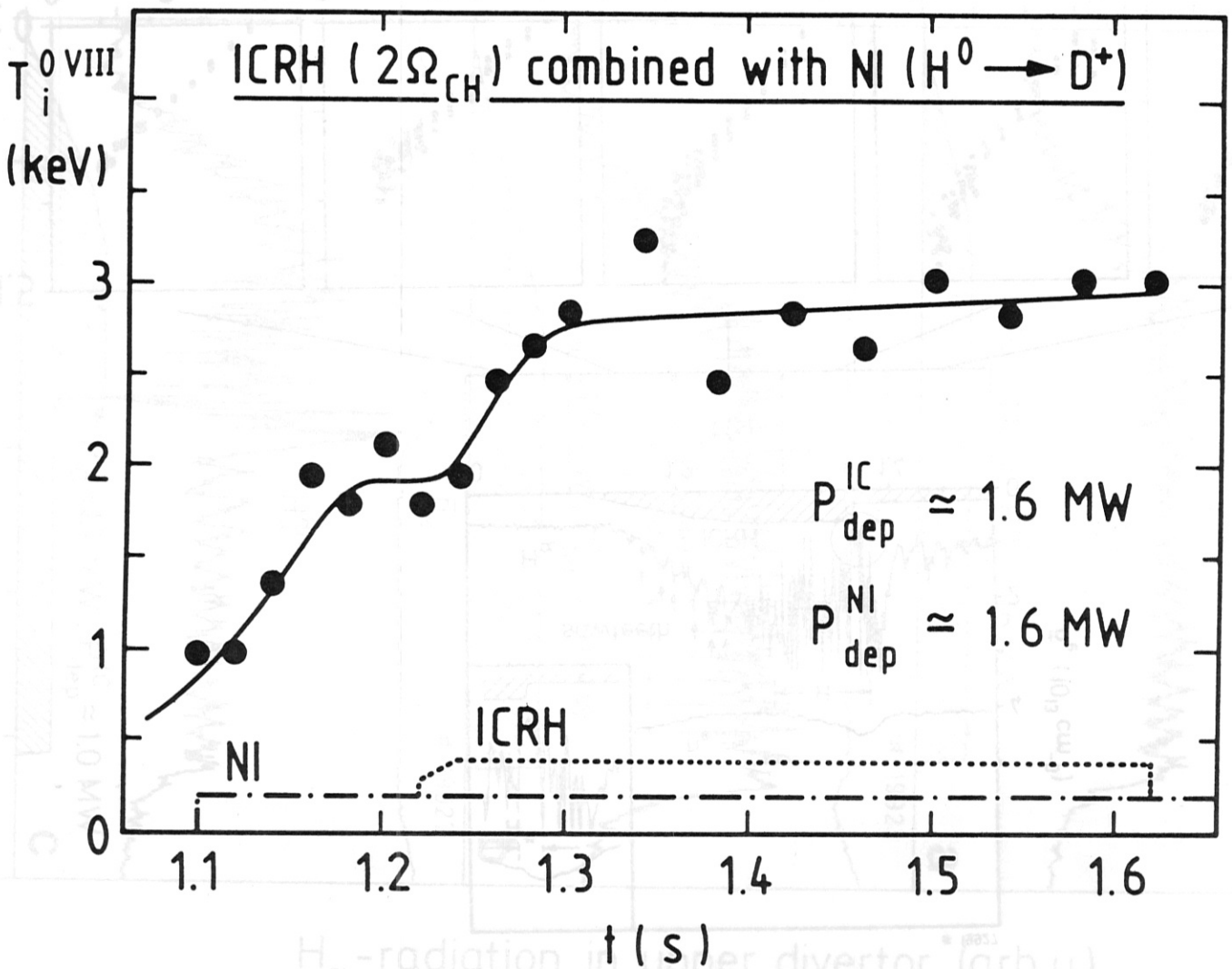

Fig. 18b

IPP3- STM 498- 85

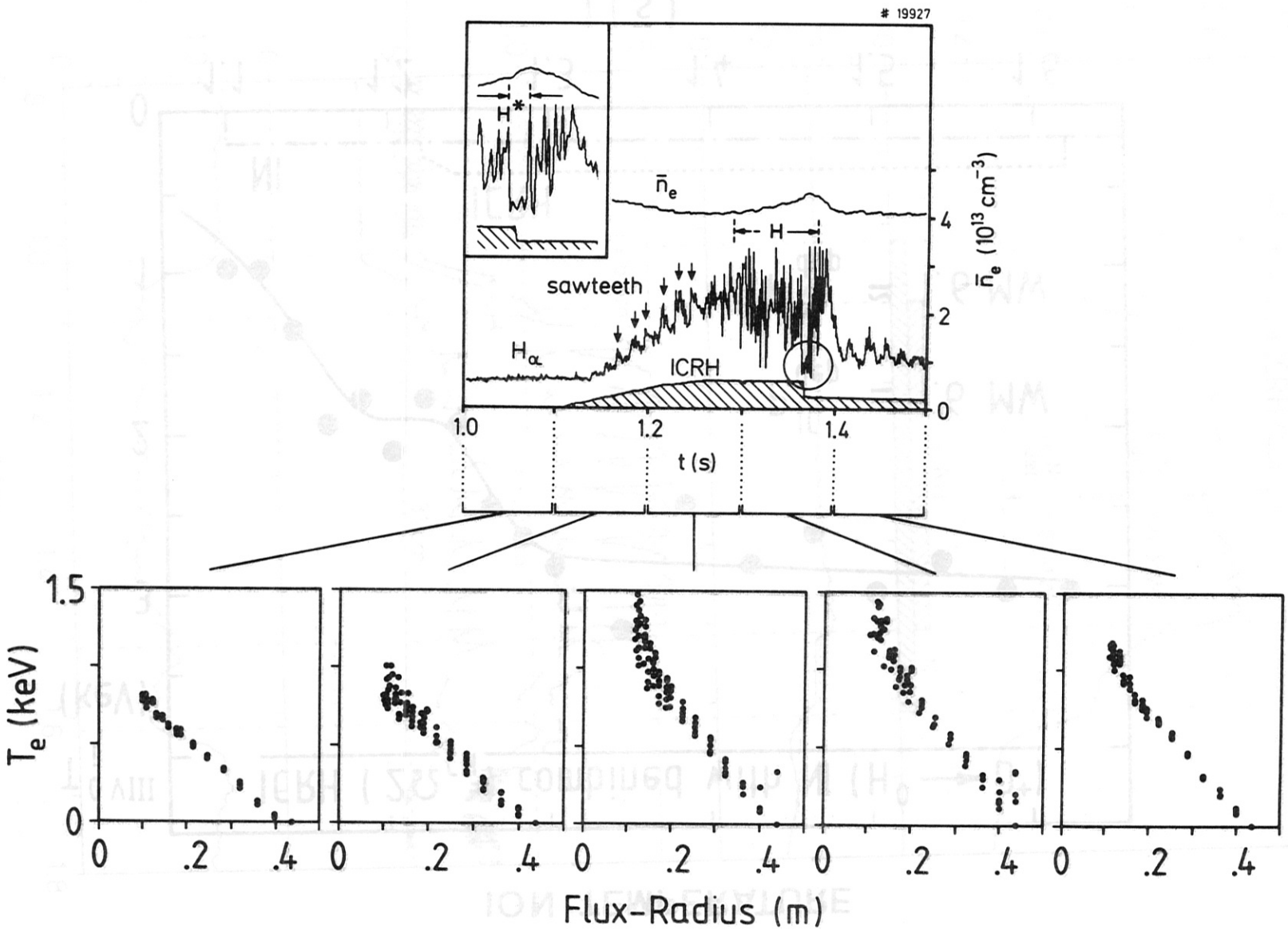
19927
H*
$\bar{n}_e$
H
sawteeth
H_α
ICRH
$\bar{n}_e$ (10^{13} cm^{-3})
4
2
0
1.0
1.2
1.4
t (s)
T_e (keV)
1.5
0
0
.2
.4
Flux-Radius (m)
IPP3- STM 003- 87

Fig. 19

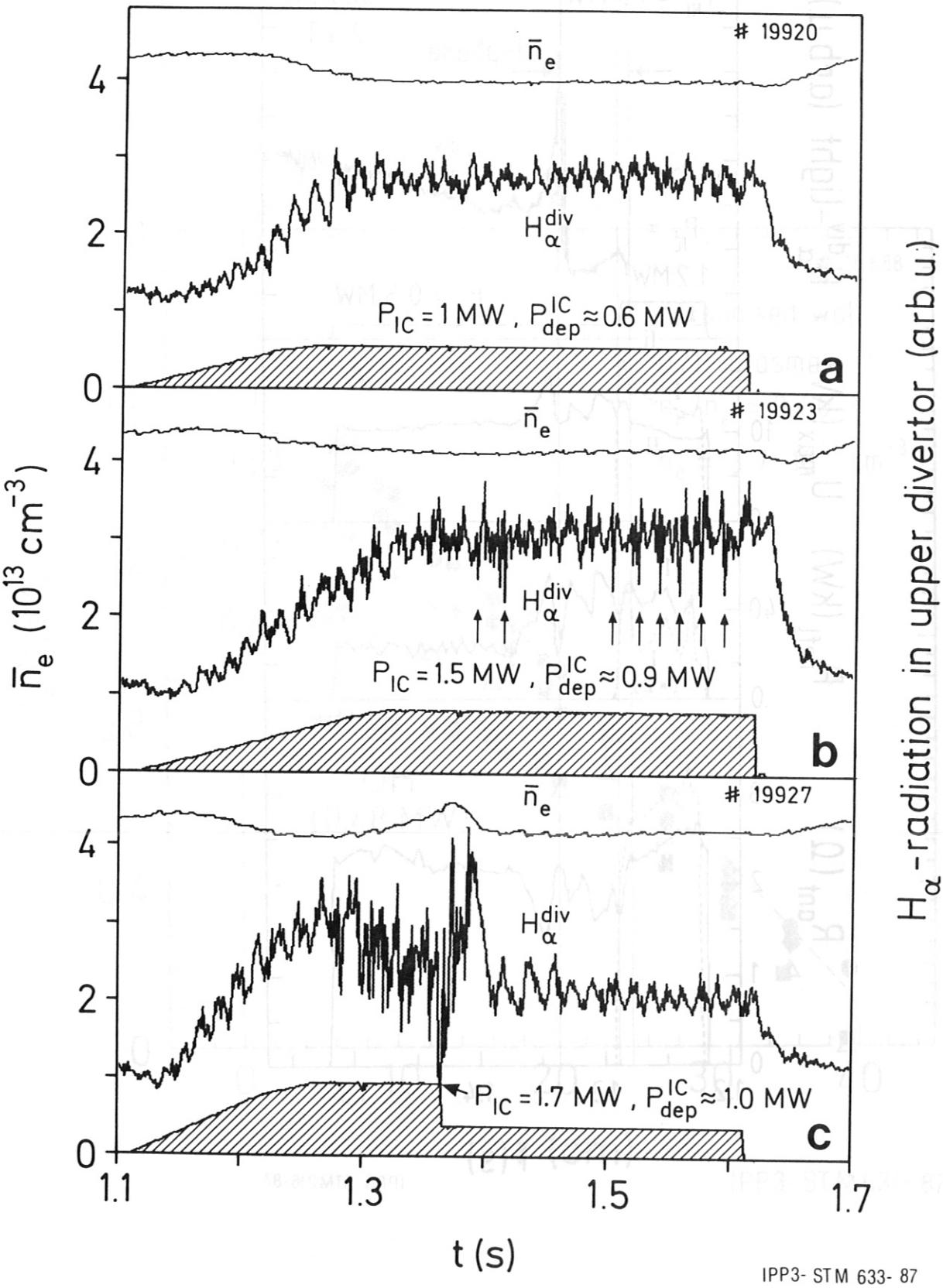

IPP3- STM 633- 87

Fig. 20

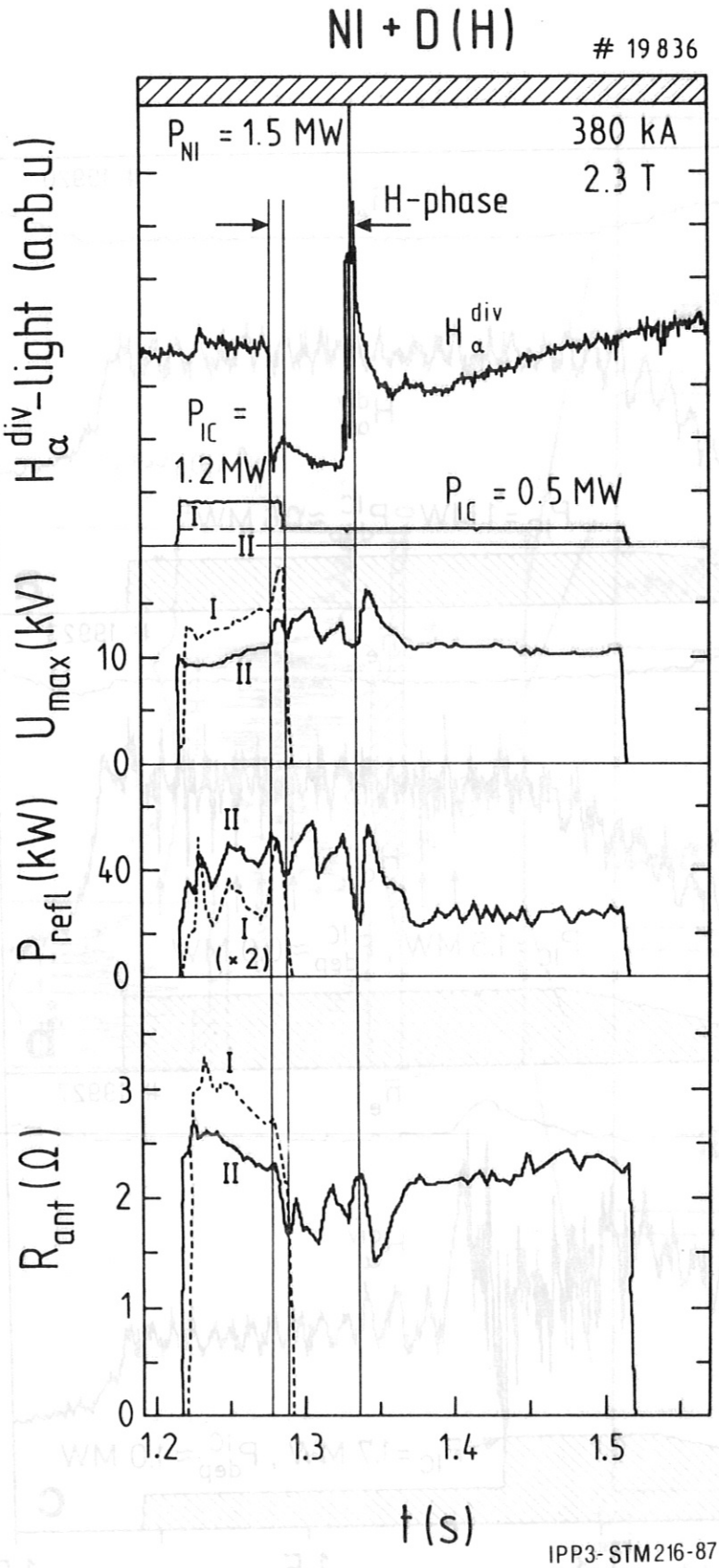
NI + D(H)
# 19836
P_NI = 1.5 MW
380 kA
2.3 T
H-phase
H_α^div
P_IC = 1.2 MW
P_IC = 0.5 MW
I
II
H_α^div-light (arb.u.)
U_max (kV)
10
0
P_refl (kW)
40
0
(×2)
R_ant (Ω)
3
2
1
0
1.2
1.3
1.4
1.5
t (s)
IPP3-STM216-87

Fig. 21

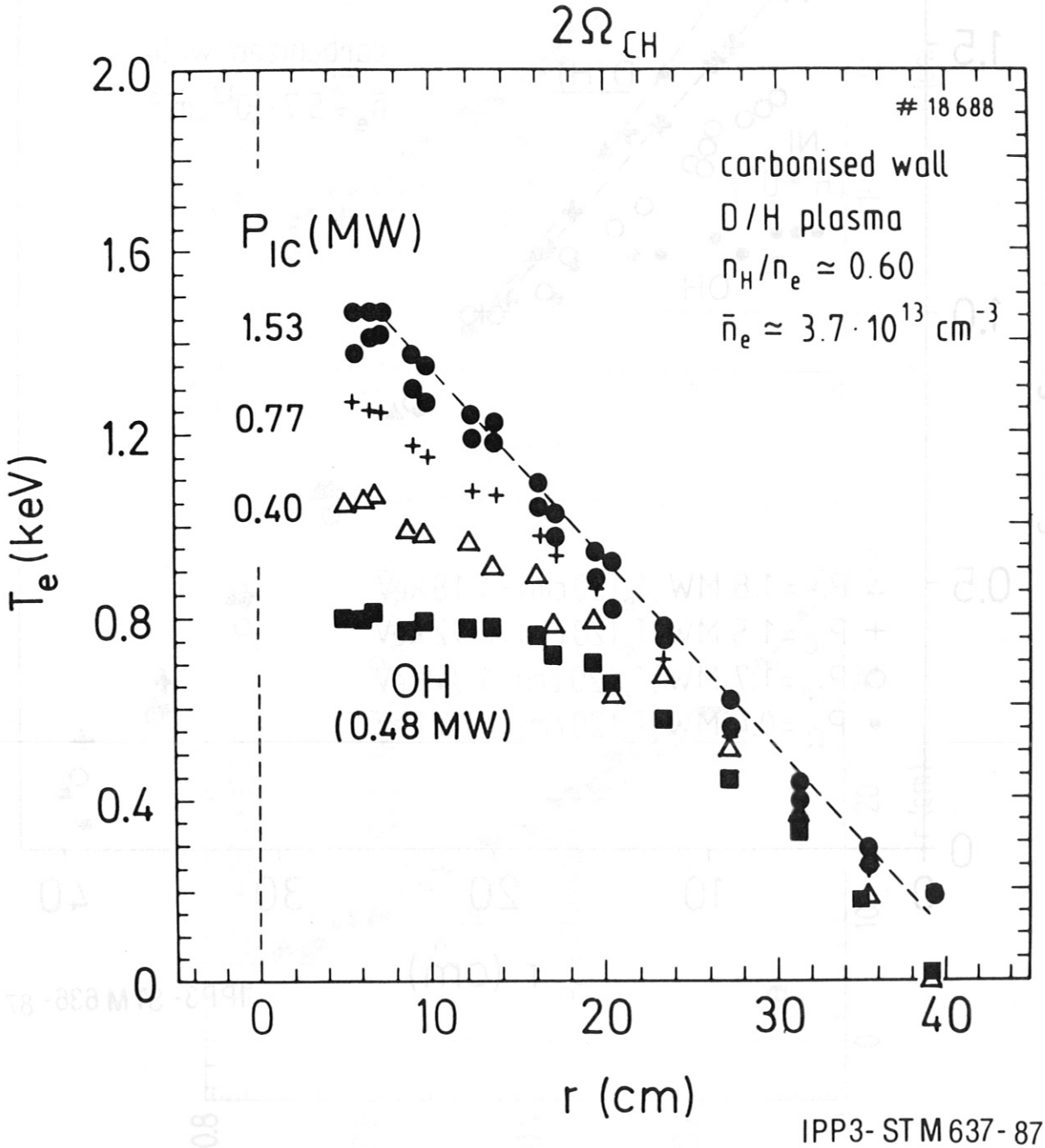
2Ω CH
18688
carbonised wall
D/H plasma
$n_H/n_e \simeq 0.60$
$\bar{n}_e \simeq 3.7 \cdot 10^{13}$ cm^{-3}
P_{IC}(MW)
1.53
0.77
0.40
OH
(0.48 MW)
T_e (keV)
r (cm)
2.0
1.6
1.2
0.8
0.4
0
0
10
20
30
40
IPP3-STM637-87

Fig. 22

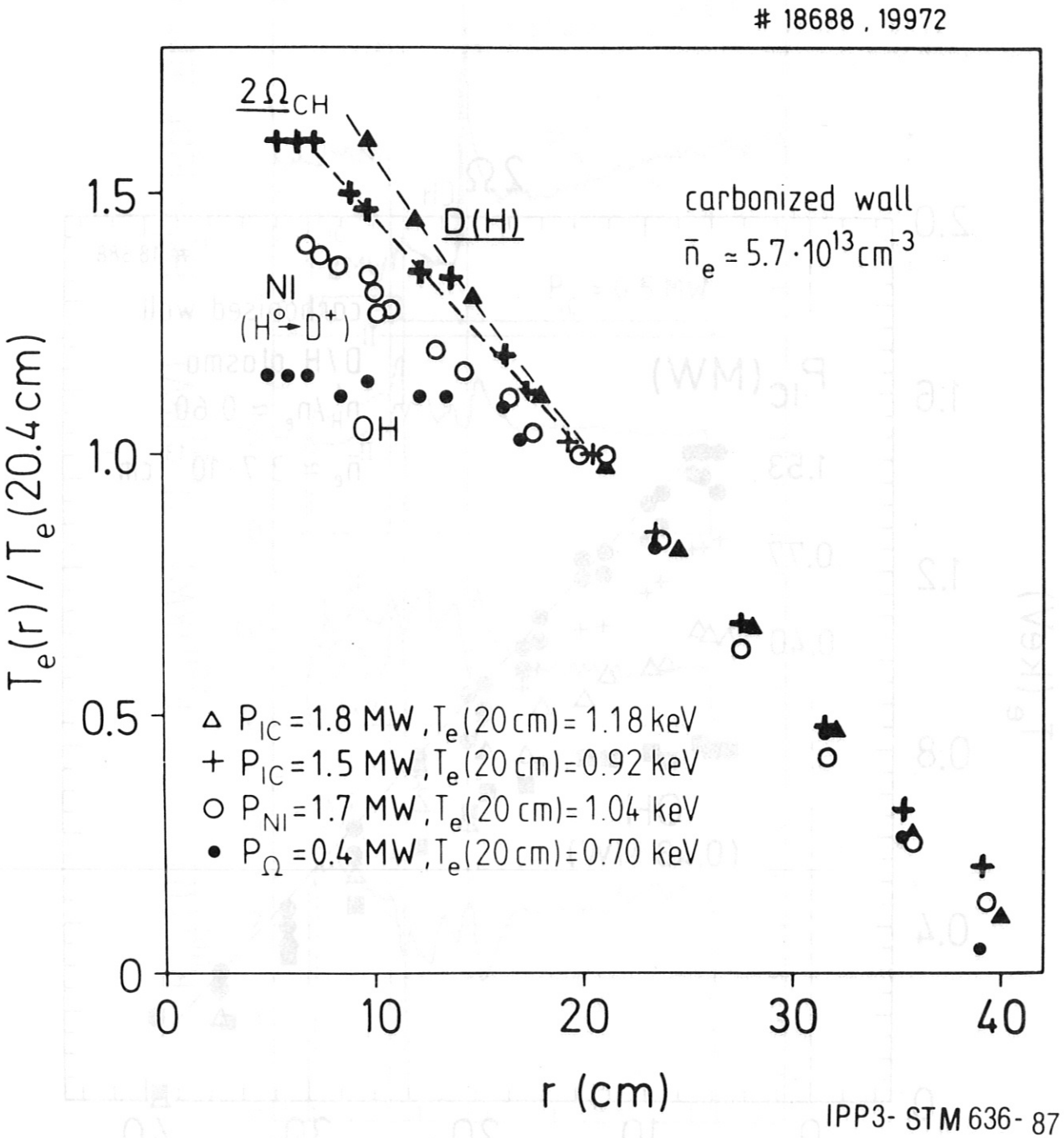
18688 , 19972
2 Ω CH
D(H)
NI
(H° → D⁺)
OH
carbonized wall
$\bar{n}_e \simeq 5.7 \cdot 10^{13} cm^{-3}$
△ P_{IC} = 1.8 MW , T_e(20 cm) = 1.18 keV
+ P_{IC} = 1.5 MW , T_e(20 cm) = 0.92 keV
○ P_{NI} = 1.7 MW , T_e(20 cm) = 1.04 keV
• P_{Ω} = 0.4 MW , T_e(20 cm) = 0.70 keV
$T_e(r) / T_e(20.4\,cm)$
r (cm)
0
0.5
1.0
1.5
0
10
20
30
40
IPP3- STM 636- 87

Fig. 23

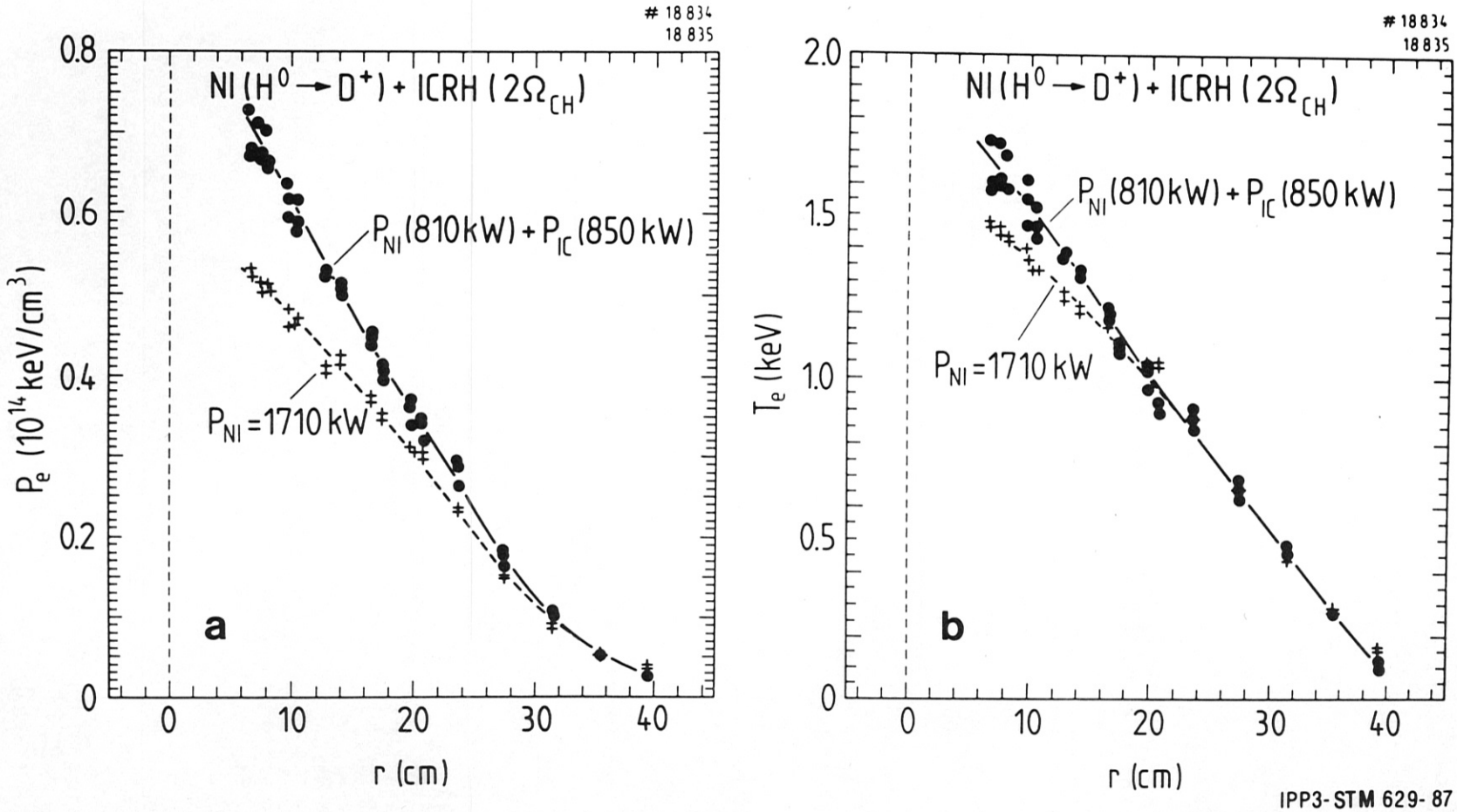
#18834
18835
NI (H⁰ → D⁺) + ICRH (2Ω_CH)
P_NI (810 kW) + P_IC (850 kW)
P_NI = 1710 kW
P_e (10¹⁴ keV/cm³)
T_e (keV)
r (cm)
a
b
IPP3-STM 629-87

Fig. 24